

# Charge and pairing dynamics in the attractive Hubbard model: mode coupling and the validity of linear-response theory

Jörg Büneemann<sup>1,2</sup> and Götz Seibold<sup>1</sup>

<sup>1</sup>*Institut für Physik, BTU Cottbus-Senftenberg, P.O. Box 101344, 03013 Cottbus, Germany*

<sup>2</sup>*Fakultät Physik, Technische Universität Dortmund, 44227 Dortmund, Germany*

(Dated: March 12, 2022)

Pump-probe experiments have turned out as a powerful tool in order to study the dynamics of competing orders in a large variety of materials. The corresponding analysis of the data often relies on standard linear-response theory generalized to non-equilibrium situations. Here we examine the validity of such an approach within the attractive Hubbard model for which the dynamics of pairing and charge-density wave orders is computed using the time-dependent Hartree-Fock approximation (TDHF). Our calculations reveal that the ‘linear-response assumption’ is justified for small to moderate non-equilibrium situations (i.e., pump pulses) when the symmetry of the pump-induced state differs from that of the external field. This is the case, when we consider the pairing response in a charge-ordered state or the charge-order response in a superconducting state. The situation is very different when the non-equilibrium state and the external probe field have the same symmetry. In this case, we observe significant changes of the response in magnitude but also due to mode coupling when moving away from an equilibrium state, indicating the failure of the linear-response assumption.

PACS numbers:

## I. INTRODUCTION

In many experiments that are carried out in solid-state physics, one measures so called ‘response functions’. Such a function provides information on the *linear* response of a given observable to a small time (or frequency) dependent external perturbation. When a system is in its ground state (or, at finite temperature, in thermal equilibrium) the well-known ‘Kubo formula’<sup>1,2</sup> identifies the response functions as retarded two-particle Greens functions.<sup>3</sup> Important examples are the magnetic or the charge susceptibilities as well as the optical conductivity.

In recent years, the development of ultrafast laser sources made it possible to measure response functions not only in equilibrium. Such measurements are usually denoted as ‘pump-and-probe experiments’ because a large pump pulse first drives the system out of equilibrium before a small probe pulse measures the usual response function. This kind of technique has been successfully applied to investigate the dynamics of electronic and phononic processes in high- $T_c$  superconductors<sup>4–11</sup> in order to elucidate the ‘glue’ for the Cooper pair binding. This can be achieved e.g. by a pump pulse through impulsive stimulated Raman scattering which induces an out-of-equilibrium condensate for which coupled excitations can be measured by a successive optical probe<sup>12,13</sup>. Moreover, pump and probe methods have been used to study the out-of-equilibrium dynamics of competing order parameter in correlated systems as e.g. the dynamics of spin and charge orders in nickelates<sup>14,15</sup> or the interplay of charge-density wave and superconducting orders in high- $T_c$  cuprates<sup>16,17</sup> (for a review see Refs. [18,19] and references therein).

It is obvious that the calculation of a non-equilibrium

response function is even more challenging than that of its equilibrium counterpart. In this regard, different schemes have been employed to generalize the Kubo formula to out-of-equilibrium situations<sup>20–22</sup> which have been critically analyzed in the context of the optical conductivity.<sup>23</sup>

In general, the dynamics of a quantum system can be obtained from non-equilibrium Green’s function (NEGF) techniques which requires the solution of the so-called Keldysh-Kadanoff-Baym equations.<sup>24,25</sup> For interacting systems these are usually decoupled within a conserving approximation. For weak to moderate interactions the lowest order corresponds to the time-dependent Hartree-Fock approximation (TDHF) which will be employed in the present paper. We note that in case of strongly correlated systems also the dynamical mean-field theory<sup>26</sup> and the Gutzwiller approximation<sup>27–29</sup> have been generalized to the description of time-dependent phenomena. On the other hand, in symmetry-broken systems the order parameter dynamics can be phenomenologically described through time-dependent Ginzburg-Landau theory (see e.g. Ref. [18]) which among others has been successfully applied to the description of spin and charge order dynamics in nickelates.<sup>14,15,30</sup>

In this work, it is our aim to analyze the dynamics of competing orders in a given microscopic model which, as mentioned above, we accomplish within the TDHF.<sup>31,32</sup> This method can be used for the study of time development near and away from equilibrium. It therefore allows us the unbiased investigation of pump-and-probe situations without any linear-response assumption. Moreover, in the small-amplitude limit the TDHF reduces to the well-known ‘random-phase approximation’<sup>31,32</sup> which corresponds to linear-response theory so that our approach allows for exploring the validity of the Kubo for-

mula in out-of equilibrium situations of competing orders. The major drawback of the Hartree-Fock approximation is its use of single-particle wave functions which can lead to flawed results already for the ground-state properties when correlation effects become important.

Our investigations will focus on the attractive Hubbard model which is one of the simplest systems that shows non-trivial symmetry-broken phases already within the Hartree-Fock approximation. For weak on-site attraction and at zero temperature the dominating instability is that to a standard BCS superconductor with isotropic s-wave order parameter. For a bipartite lattice at half-filling the model has  $SO(3)$  symmetry and the SC state is degenerate with a commensurate charge-density wave. Without additional long-range interactions and away from half-filling, the SC phase constitutes the ground state, i.e., it is always more stable than a charge ordered state.<sup>33</sup>

The SC order parameter dynamics of related BCS-type models has been in the focus of numerous previous studies<sup>34–37</sup> and has also been investigated for multi-band superconductivity.<sup>38</sup> In the linear-response limit<sup>39</sup> a small perturbation of the SC order parameter  $\Delta$  excites amplitude modes with an energy corresponding to the SC gap  $2\Delta$  and which are damped due to their admixture with Bogoljubov quasiparticle excitations. As a consequence the order parameter relaxation towards a constant shows an oscillatory behavior with frequency  $\Omega = 2\Delta$  and an amplitude which decays  $\sim 1/\sqrt{t}$ . Later it has been shown<sup>40</sup> that this dynamics is also obeyed beyond the linear response regime when the non-equilibrium state is in the same class as the ground state, e.g., when the non-equilibrium state is generated from a paired ground state by a sudden change of the pairing strength. In the other case, i.e., when non-equilibrium and ground state are topologically different, persistent oscillations of the order parameter occur. This can be achieved, e.g., by an initial normal state while the ground state is a superconductor.

In the present paper, we investigate the dynamics of competing orders, namely charge density wave (CDW) order and SC order, in the context of the validity of linear-response theory in a non-equilibrium situation. Thus we will also deal with a scenario where a ground and non-equilibrium state have different symmetries, namely SC and CDW or vice versa. However, since without additional interaction the ground state of the attractive Hubbard model at weak coupling is a BCS superconductor we supplement the model with a staggered charge order field, arising, e.g., from a lattice distortion, in order to realize three different ground state symmetries, i) a pure SC state, ii) a charge-ordered state, or iii) a state with both orders present. The stability and proximity of these phases makes the attractive Hubbard model an ideal playing field for the study of non-equilibrium response functions because we can combine each of the three possible symmetries of the pump-pulse induced initial state with the two relevant symmetries of a probe

pulse. Note that the attractive Hubbard model with both SC and CDW orders has recently also been investigated in the context of the visibility of the amplitude (Higgs) mode within linear (Raman) response.<sup>41</sup>

Our work is organized as follows: In Sec. II we discuss our model, the details about its treatment within TDHF, and our way of simulating pump and probe experiments. The ground-state properties of our model are discussed in Sec. III. In Sec. IV, on out-of-equilibrium dynamics, we show in detail the results for quantum-quench dynamics as well as pump-and-probe simulations. We close our presentation with concluding remarks in Sec. V. Details on our numerical minimization and the results for two tutorial toy models are deferred to three appendices.

## II. MODEL AND METHOD

In this chapter, we will present the theoretical background of our study. First, in Sec. II A, we introduce our model and derive its Hartree-Fock energy functional. Second, in Sec. II B, the TDHF equations for our model are derived. Third, in Sec. II C, we explain how we will simulate pump and probe experiments.

### A. Hamiltonian and ground-state energy functional

We consider the attractive (‘negative  $U$ ’) Hubbard model defined by

$$\hat{H}_H = \hat{H}_0 - U \sum_{\mathbf{i}} \hat{n}_{\mathbf{i},\uparrow} \hat{n}_{\mathbf{i},\downarrow} \quad (U \geq 0), \quad (1)$$

$$\hat{H}_0 = \sum_{\mathbf{i},\mathbf{j},\sigma} t_{\mathbf{i},\mathbf{j}} \hat{c}_{\mathbf{i},\sigma}^\dagger \hat{c}_{\mathbf{j},\sigma} = \sum_{\mathbf{k},\sigma} \varepsilon_{\mathbf{k}} \hat{c}_{\mathbf{k},\sigma}^\dagger \hat{c}_{\mathbf{k},\sigma} \quad (2)$$

where  $\mathbf{i}, \mathbf{j}$  are lattice-site vectors,  $\sigma$  the spin index,  $\hat{n}_{\mathbf{i},\sigma} \equiv \hat{c}_{\mathbf{i},\sigma}^\dagger \hat{c}_{\mathbf{i},\sigma}$ , and  $\mathbf{k}$  a wave vector in the first Brillouin zone. For simplicity, we assume a bipartite lattice with sublattices  $A/B$  that can be defined with a nesting vector  $\mathbf{Q}$  via

$$e^{i\mathbf{Q} \cdot \mathbf{i}} = \begin{cases} +1 & \text{if } \mathbf{i} \in A \\ -1 & \text{if } \mathbf{i} \in B \end{cases}. \quad (3)$$

We further assume that the hopping parameters  $t_{\mathbf{i},\mathbf{j}}$  are non-zero only when  $\mathbf{i}$  and  $\mathbf{j}$  belong to different sublattices. This leads to

$$\varepsilon_{\mathbf{k}+\mathbf{Q}} = -\varepsilon_{\mathbf{k}} \quad (4)$$

for the dispersion relation in (2).

In the following, we want to study states which may include local pairing as well as charge order. On a mean-field level, i.e., evaluated with a single-particle product wave function, the expectation value of the (local) two-particle interaction in (1) then has the form

$$\langle \hat{n}_{\mathbf{i},\uparrow} \hat{n}_{\mathbf{i},\downarrow} \rangle = \langle \hat{n}_{\mathbf{i},\uparrow} \rangle \langle \hat{n}_{\mathbf{i},\downarrow} \rangle + \langle \hat{c}_{\mathbf{i},\uparrow}^\dagger \hat{c}_{\mathbf{i},\downarrow}^\dagger \rangle \langle \hat{c}_{\mathbf{i},\downarrow} \hat{c}_{\mathbf{i},\uparrow} \rangle \quad (5)$$

where we impose the charge- and pair-density fields as

$$\langle \hat{c}_{i,\uparrow}^\dagger \hat{c}_{i,\downarrow}^\dagger \rangle = \Delta_0 + e^{i\mathbf{Q} \cdot \mathbf{i}} \Delta_{\mathbf{Q}} , \quad (6)$$

$$\langle \hat{n}_{i,\sigma} \rangle = n_0 + e^{i\mathbf{Q} \cdot \mathbf{i}} n_{\mathbf{Q}} . \quad (7)$$

Here,  $\Delta_0$ ,  $n_0$ ,  $n_{\mathbf{Q}}$ , and  $\Delta_{\mathbf{Q}}$  are lattice-site independent numbers.

In real materials, a charge order can be stabilized by a static distortion of the lattice. To simulate this effect we allow for a external ‘charge-order field’

$$\hat{H}_{\text{co}} \equiv \frac{\alpha_{\mathbf{Q}}}{2} \sum_{\mathbf{i},\sigma} e^{i\mathbf{Q} \cdot \mathbf{i}} \hat{n}_{\mathbf{i},\sigma} \quad (8)$$

and study in the following the Hamiltonian

$$\hat{H} \equiv \hat{H}_{\text{H}} + \hat{H}_{\text{co}} . \quad (9)$$

In a superconducting phase the total particle number is not conserved but its expectation value has to be fixed by means of a chemical potential  $\mu$ . Hence we work with  $\hat{K} \equiv \hat{H} - \mu \hat{N}$  instead of  $\hat{H}$ . The expectation value of  $\hat{K}$  is given as

$$\begin{aligned} \frac{\langle \hat{K} \rangle}{L} &= \frac{1}{L} \sum_{\mathbf{k},\sigma} (\varepsilon_{\mathbf{k}} - \mu) \langle \hat{c}_{\mathbf{k},\sigma}^\dagger \hat{c}_{\mathbf{k},\sigma} \rangle \\ &\quad - U \left( (n_{\mathbf{Q}})^2 + |\Delta_0|^2 + |\Delta_{\mathbf{Q}}|^2 \right) + \alpha_{\mathbf{Q}} n_{\mathbf{Q}} . \end{aligned} \quad (10)$$

Note that in this expression we have dropped the constant energy shift  $Un_0^2$  on the right hand side. The order parameters in (10) can be calculated in momentum space with

$$\Delta_0 = \langle \hat{\Delta}_0 \rangle , \quad \hat{\Delta}_0 \equiv \frac{1}{L} \sum_{\mathbf{k}} \hat{c}_{\mathbf{k},\uparrow}^\dagger \hat{c}_{-\mathbf{k},\downarrow}^\dagger , \quad (11)$$

$$\Delta_{\mathbf{Q}} = \langle \hat{\Delta}_{\mathbf{Q}} \rangle , \quad \hat{\Delta}_{\mathbf{Q}} \equiv \frac{1}{L} \sum_{\mathbf{k}} \hat{c}_{\mathbf{k},\uparrow}^\dagger \hat{c}_{-\mathbf{k}-\mathbf{Q},\downarrow}^\dagger , \quad (12)$$

$$n_{\mathbf{Q}} = \langle \hat{n}_{\mathbf{Q}} \rangle , \quad \hat{n}_{\mathbf{Q}} \equiv \frac{1}{2L} \sum_{\mathbf{k},\sigma} \hat{c}_{\mathbf{k},\sigma}^\dagger \hat{c}_{\mathbf{k}+\mathbf{Q},\sigma} . \quad (13)$$

With the nesting vector  $\mathbf{Q}$ , we may split the Brillouin zone  $\mathcal{B}$  into two parts  $\mathcal{B} = \mathcal{B}_0 \cup \mathcal{B}_{\mathbf{Q}}$  such that for each  $\mathbf{k}$  we have either  $\mathbf{k} \in \mathcal{B}_0$  or  $\mathbf{k} \in \mathcal{B}_{\mathbf{Q}}$ ,  $\mathbf{k} - \mathbf{Q} \in \mathcal{B}_0$ . For convenience,  $\mathcal{B}_0$  is chosen such that, with  $\mathbf{k} \in \mathcal{B}_0$  it is also  $-\mathbf{k} \in \mathcal{B}_0$ . To get rid of the anomalous expectation values in (11),(12) we introduce the following canonical transformation

$$\hat{d}_{\mathbf{k},1}^\dagger = \hat{c}_{\mathbf{k},\uparrow}^\dagger , \quad (14)$$

$$\hat{d}_{\mathbf{k},2}^\dagger = \hat{c}_{-\mathbf{k},\downarrow}^\dagger , \quad (15)$$

$$\hat{d}_{\mathbf{k},3}^\dagger = \hat{c}_{\mathbf{k}+\mathbf{Q},\uparrow}^\dagger , \quad (16)$$

$$\hat{d}_{\mathbf{k},4}^\dagger = \hat{c}_{-\mathbf{k}-\mathbf{Q},\downarrow}^\dagger , \quad (17)$$

for all  $\mathbf{k} \in \mathcal{B}_0$ . With these operators, we may write the operators in (11)-(13) as

$$\hat{\Delta}_0 = \frac{1}{L} \sum_{\mathbf{k} \in \mathcal{B}_0} \left( \hat{d}_{\mathbf{k},1}^\dagger \hat{d}_{\mathbf{k},2} + \hat{d}_{\mathbf{k},3}^\dagger \hat{d}_{\mathbf{k},4} \right) , \quad (18)$$

$$\hat{\Delta}_{\mathbf{Q}} = \frac{1}{L} \sum_{\mathbf{k} \in \mathcal{B}_0} \left( \hat{d}_{\mathbf{k},1}^\dagger \hat{d}_{\mathbf{k},4} + \hat{d}_{\mathbf{k},3}^\dagger \hat{d}_{\mathbf{k},2} \right) , \quad (19)$$

$$\begin{aligned} \hat{n}_{\mathbf{Q}} &= \frac{1}{2L} \sum_{\mathbf{k} \in \mathcal{B}_0} \sum_{j=0}^1 (-1)^j \\ &\quad \times \left( \hat{d}_{\mathbf{k},1+j}^\dagger \hat{d}_{\mathbf{k},3+j} + \hat{d}_{\mathbf{k},3+j}^\dagger \hat{d}_{\mathbf{k},1+j} \hat{\Delta}_0 \right) . \end{aligned} \quad (20)$$

For the single particle energies in (10) we obtain

$$\begin{aligned} \sum_{\mathbf{k},\sigma} \varepsilon_{\mathbf{k}} \langle \hat{c}_{\mathbf{k},\sigma}^\dagger \hat{c}_{\mathbf{k},\sigma} \rangle &= \sum_{\mathbf{k} \in \mathcal{B}_0} \varepsilon_{\mathbf{k}} \left( \langle \hat{d}_{\mathbf{k},1}^\dagger \hat{d}_{\mathbf{k},1} \rangle - \langle \hat{d}_{\mathbf{k},2}^\dagger \hat{d}_{\mathbf{k},2} \rangle \right. \\ &\quad \left. - \langle \hat{d}_{\mathbf{k},3}^\dagger \hat{d}_{\mathbf{k},3} \rangle + \langle \hat{d}_{\mathbf{k},4}^\dagger \hat{d}_{\mathbf{k},4} \rangle \right) , \end{aligned} \quad (21)$$

$$\begin{aligned} \mu \sum_{\mathbf{k},\sigma} \langle \hat{c}_{\mathbf{k},\sigma}^\dagger \hat{c}_{\mathbf{k},\sigma} \rangle &= \mu \sum_{\mathbf{k} \in \mathcal{B}_0} \left( \langle \hat{d}_{\mathbf{k},1}^\dagger \hat{d}_{\mathbf{k},1} \rangle - \langle \hat{d}_{\mathbf{k},2}^\dagger \hat{d}_{\mathbf{k},2} \rangle \right. \\ &\quad \left. \langle \hat{d}_{\mathbf{k},3}^\dagger \hat{d}_{\mathbf{k},3} \rangle - \langle \hat{d}_{\mathbf{k},4}^\dagger \hat{d}_{\mathbf{k},4} \rangle \right) , \end{aligned} \quad (22)$$

With equations (10), (18)-(22), we have determined the energy

$$\langle \hat{K} \rangle \equiv E(\tilde{\rho}) \quad (23)$$

as a function of the single-particle density matrix  $\tilde{\rho}$ . This matrix is diagonal with respect to  $\mathbf{k}$  and therefore determined by the four-dimensional matrices

$$\rho_{\mathbf{k};\gamma,\gamma'} = \langle \hat{d}_{\mathbf{k},\gamma}^\dagger \hat{d}_{\mathbf{k},\gamma'} \rangle , \quad (24)$$

for each  $\mathbf{k} \in \mathcal{B}_0$ .

## B. Out of equilibrium dynamics

The time dependence of the single-particle density matrix  $\tilde{\rho}$  is governed by the well-known differential equation<sup>29,31,32</sup>

$$i\dot{\tilde{\rho}} = [\tilde{h}, \tilde{\rho}] , \quad (25)$$

where  $\tilde{h}$  is also diagonal with respect to  $\mathbf{k}$  and defined as

$$\tilde{h}_{\mathbf{k};\gamma,\gamma'} \equiv \frac{\partial}{\partial \rho_{\mathbf{k};\gamma',\gamma}} E(\tilde{\rho}) . \quad (26)$$

Explicitly,  $\tilde{h}_{\mathbf{k};\gamma,\gamma'}$  is given by the four-dimensional matrix

$$\tilde{h}_{\mathbf{k}} = \begin{pmatrix} \varepsilon_{\mathbf{k}} - \mu & -\eta_{\text{sc}} & -\eta_{\text{co}} & -\delta\eta_{\text{sc}} \\ -\eta_{\text{sc}}^* & -\varepsilon_{\mathbf{k}} + \mu & -\delta\eta_{\text{sc}}^* & \eta_{\text{co}} \\ -\eta_{\text{co}} & -\delta\eta_{\text{sc}} & -\varepsilon_{\mathbf{k}} - \mu & -\eta_{\text{sc}} \\ -\delta\eta_{\text{sc}}^* & \eta_{\text{co}} & -\eta_{\text{sc}}^* & \varepsilon_{\mathbf{k}} + \mu \end{pmatrix} , \quad (27)$$

with the four eigenvalues

$$E_{\pm}^2(\mathbf{k}) = \delta\eta_{\text{sc}}^2 + \varepsilon_{\mathbf{k}}^2 + \mu^2 + \eta_{\text{sc}}^2 + \eta_{\text{co}}^2 \pm 2\sqrt{\varepsilon_{\mathbf{k}}^2(\delta\eta_{\text{sc}}^2 + \mu^2) + (\delta\eta_{\text{sc}}\eta_{\text{sc}} + \mu\eta_{\text{co}})^2}. \quad (28)$$

Here, the ‘fields’

$$\eta_{\text{sc}} = U\Delta_0, \quad (29)$$

$$\eta_{\text{co}} = Un_{\mathbf{Q}} - \alpha_{\mathbf{Q}}/2, \quad (30)$$

$$\delta\eta_{\text{sc}} = U\Delta_{\mathbf{Q}}, \quad (31)$$

are, through (11)-(20), time-dependent functions that need to be determined self-consistently. The calculation of these fields is simplified significantly by our  $A/B$  lattice structure and the resulting property (4) of the dispersion relation. It allows us to replace all momentum-space integrals by energy integrals, e.g.,

$$\Delta_0 = \int d\varepsilon D(\varepsilon) \left( \langle \hat{d}_{\varepsilon,1}^\dagger \hat{d}_{\varepsilon,2} \rangle + \langle \hat{d}_{\varepsilon,3}^\dagger \hat{d}_{\varepsilon,4} \rangle \right), \quad (32)$$

where we introduced the (bare) density of states

$$D(\varepsilon) = \frac{1}{L} \sum_{\mathbf{k} \in \mathcal{B}_0} \delta(\varepsilon - \varepsilon_{\mathbf{k}}). \quad (33)$$

In the following, we will work with the semi-elliptic density of states

$$D(\varepsilon) = \frac{2}{\pi J^2} \sqrt{J^2 - \varepsilon^2} \quad (\varepsilon \leq 0), \quad (34)$$

in which  $J$  sets the energy scale of our model. We note in passing that in test calculations we observed only minor quantitative changes of the results when we replace (34) by the more realistic density of states of a two-dimensional square lattice with nearest-neighbor hopping.

Since  $\tilde{\rho}$  and  $\tilde{h}$  are block diagonal with respect to  $\mathbf{k}$  (or from now on  $\varepsilon$ ), we need to solve the four differential equations

$$i\dot{\tilde{\rho}}_\varepsilon = [\tilde{h}_\varepsilon, \tilde{\rho}_\varepsilon] \quad (35)$$

for each  $\varepsilon$ . It is clear that, in our numerical solution, we have to discretize the energy interval  $-J \leq \varepsilon \leq 0$  and solve (35) for a finite number  $N_{\text{disk}}$  of energy points  $\varepsilon_i$ . We found a number of  $N_{\text{disk}} = 10^4$  to be sufficiently accurate.

The differential equations (35) cannot be solved analytically because the fields in (27) are unknown time-dependent functions. Hence we use the numerical Adams–Bashforth<sup>42</sup> method to 4-th order. After each time-step, we have to recalculate the fields (11)-(13).

It is worth mentioning that the total particle number, although no conserved quantity in the BCS approximation due to the breaking of  $U(1)$  symmetry, is conserved in the time evolution described by Eq. (25). Only numerical errors could lead to an error in the particle number as a function of time. This error, however, was found to be negligible for the time periods which we are interested in.

### C. Simulation of pump-and-probe experiments

In a typical pump-and-probe experiment, the system under investigation is in its ground state  $|\phi_0\rangle$  (or in equilibrium at finite temperatures) at some time  $t = -T$ . Then, in the time interval  $t \in (-T, 0)$ , a ‘large’ pump field is applied that drives the system into some non-equilibrium state  $|\phi(0)\rangle$  at time  $t = 0$ . The further time evolution  $|\phi(t)\rangle$  of this state follows from a solution of the time-dependent Schrödinger equation for the Hamiltonian  $\hat{H}$  of the system (in our case  $\hat{K}$ ).

One is interested in the response of the system to a ‘small’ probe pulse of the form

$$\hat{V} = \sin(\omega t)\Omega(t)\hat{A} \equiv f(t)\hat{A} \quad (36)$$

that is applied at times  $t > 0$ . Here,  $\Omega(t)$  is an envelope function and  $\hat{A}$  some operator, e.g.,

$$\hat{A} = \hat{\Delta}_0 \text{ or } \hat{A} = \hat{n}_{\mathbf{Q}}, \quad (37)$$

i.e., the operators that describe the the SC amplitude or the charge modulation. The wave function  $|\phi_{\text{p}}(t)\rangle$ , in the presence of the probe pulse, differs from  $|\phi(t)\rangle$  and so does the expectation value of  $\hat{A}$ . Hence, we may define

$$\delta A(t) \equiv \langle \hat{A} \rangle_{\phi_{\text{p}}(t)} - \langle \hat{A} \rangle_{\phi(t)} \quad (38)$$

as a measure for the impact of  $\hat{V}$  on the observable  $\hat{A}$ .

Without the pump pulse,  $\delta A(t)$  is usually calculated by means of the Kubo formula<sup>1,2</sup>

$$\delta A(t) = \int_0^t dt' \chi_{A,A}(t, t') f(t') \quad (39)$$

with the (retarded) Green’s function

$$\chi_{A,A}(t, t') \equiv -i\theta(t - t') \langle \phi(0) | [\hat{A}_{\text{I}}(t), \hat{A}_{\text{I}}(t')] | \phi(0) \rangle \quad (40)$$

where  $\hat{A}_{\text{I}}(t) = e^{i\hat{H}t} \hat{A} e^{-i\hat{H}t}$  is the interaction representation of  $\hat{A}$  (i.e.,  $\hat{H}$  is defined *without* the probe pulse). Note that, in a linear-response approximation, Eqs. (39),(40) are equally valid if  $|\phi(0)\rangle$  is the excited state induced by the pump pulse. However, the full two-time response function  $\chi_{A,A}(t, t')$  is needed here, instead of  $\chi_{A,A}(t - t')$  when the perturbation is applied to the ground state. In order to show this, we introduce the eigenstates  $|n\rangle$  and energies  $E_n$  of  $\hat{H}$  and the expansion

$$|\phi(0)\rangle = \sum_m \varphi_m |m\rangle \quad (41)$$

of the initial state. With these, we can write, e.g., the first part of the commutator in (40) as

$$\begin{aligned} & \langle \phi(0) | \hat{A}_{\text{H}}(t) \cdot \hat{A}_{\text{H}}(t') | \phi(0) \rangle \\ &= \sum_{m, m', n} \varphi_m^* \varphi_{m'} A_{m,n} A_{n,m'} e^{-iE_n(t-t')} e^{iE_m t} e^{-iE_{m'} t'}, \end{aligned} \quad (42)$$

$$A_{m,n} \equiv \langle m | \hat{A} | n \rangle. \quad (43)$$

Obviously, this quantity is a function of  $t - t'$  only when  $m = m'$ , i.e., when  $|\phi(0)\rangle$  is an eigenstate of  $\hat{H}$ . The (non equilibrium) Greens function therefore has unusual properties as becomes clear from the equivalent of a Lehmann representation: First, we can perform a Fourier transform of (40) with respect to  $\tau \equiv t - t'$  while explicitly keeping the response time  $t$

$$\chi_{A,A}(\omega, t) = \sum_{n,m,m'} \varphi_m^* \varphi_{m'} e^{i(E_m - E_{m'})t} \quad (44)$$

$$\times \left[ \frac{A_{mn} A_{nm'}}{\omega - E_{n,m} + i\delta} - \frac{A_{mn} A_{nm'}}{\omega + E_{n,m} + i\delta} \right],$$

where  $E_{n,m} \equiv E_n - E_m$ . Upon further defining a ‘long-time’ response average<sup>21</sup>

$$\tilde{\chi}_{A,A}(\omega) = \frac{1}{T'} \int_0^{T'} dt \chi_{A,A}(\omega, t) \quad (45)$$

one obtains for  $T' \rightarrow \infty$

$$\tilde{\chi}_{A,A}(\omega) \rightarrow \sum_{n,m} |\varphi_m|^2 \quad (46)$$

$$\times \left[ \frac{A_{mn} A_{nm}}{\omega - E_{n,m} + i\delta} - \frac{A_{mn} A_{nm}}{\omega + E_{n,m} + i\delta} \right].$$

This has a similar structure as the equilibrium response function but for the factor  $|\varphi_m|^2$  which describes the admixture of excited states induced by the pump pulse. It has been shown<sup>21</sup> that, for a number of cases, Eq. (46) is similar to the equilibrium response when the  $|\varphi_m|^2$  are replaced by Boltzmann weights. In this spirit we will later compare the numerically obtained response, using Eqs. (35,36), with an equilibrium response function for a non-zero effective temperature.

In equilibrium, the linear-response assumption of Eqs. (39),(40) is justified because a small perturbation will normally lead to a small response of a system that is in its stationary ground state and sufficiently far away from an instability. The situation is obviously different when the system is in a non-equilibrium state due to a pump pulse and it is not clear to what extend (39),(40) are still applicable. Since the TDHF method that we use in this work does not rely on the linear-response assumption we are able to assess its validity in pump-and-probe situations.

Relevant pump pulses are of the form given in (36)-(37). Hence, to define them, we have to specify the pulse frequency as well as the shape and duration  $T$  of the pump pulse  $\Omega(t)$ . These tunable quantities would come on top of the system parameters  $U, n, \alpha_Q$  and the probe frequency  $\omega$ . To limit the total number of such parameters, and since we are not addressing any specific experiment, we prefer to set up the initial out-of-equilibrium states not through a pump pulse but by varying the three initial fields  $\{\eta_\nu^0\} \equiv \{\eta_{sc}^0, \delta\eta_{sc}^0, \eta_{co}^0\}$  away from their ground-state values  $\eta_\nu^{gs}$ .

For a given set of initial fields  $\eta_\nu^0$  (at time  $t = 0$ ) and a given probe pulse Eq. (36) we solve Eq. (25) numerically

over a certain time period  $\Delta t$ , typically  $\Delta t = 1000/J$ . With this solution, we determine both expectation values on the r.h.s. of (38) and hereby the fluctuations  $\delta A(t)$ . Note that, for a non-Hermitian operator  $\hat{A}$  (e.g.,  $\Delta_0$ ) the latter contain both amplitude and phase contributions, i.e.,

$$|\delta A(t)|^2 = |\langle \hat{A} \rangle_{\phi_p(t)}|^2 + |\langle \hat{A} \rangle_{\phi(t)}|^2 \quad (47)$$

$$- 2|\langle \hat{A} \rangle_{\phi_p(t)}| |\langle \hat{A} \rangle_{\phi(t)}| \cos(\Phi_p(t) - \Phi_0(t))$$

where  $\Phi_{p(0)}(t)$  denotes the phase of  $\langle \hat{A} \rangle_{\phi_{p(0)}(t)}$  with (without) the probe pulse. As a measure for the impact of the probe pulse, we define

$$\langle \delta A \rangle = \frac{1}{\Delta t} \int_0^{\Delta t} dt |\delta A(t)|. \quad (48)$$

This quantity will be considered as a function of  $\omega$ , the pulse frequency in (36), where, for simplicity, we set  $\Omega(t) = \Omega_0 = 10^{-5}$ . In cases where the experiment measures only the amplitude with and without the probe pulse, in particular in connection with SC, it is also useful to define the response quantity

$$\langle \delta |\Delta_0| \rangle \equiv \frac{1}{\Delta t} \int_0^{\Delta t} dt \left| |\langle \hat{\Delta}_0 \rangle_{\phi_p(t)}| - |\langle \hat{\Delta}_0 \rangle_{\phi(t)}| \right|. \quad (49)$$

If the response occurs on top of a non-equilibrium state with  $|\langle \hat{\Delta}_0 \rangle_{\phi(t)}| \gg |\delta \Delta_0(t)|$  one can expand Eq. (48)

$$\langle \delta |\Delta_0| \rangle = \frac{1}{2\Delta t} \int_0^{\Delta t} dt \left| \delta \Delta_0(t) e^{-i\phi(t)} + \delta \Delta_0^*(t) e^{i\phi(t)} \right| \quad (50)$$

where  $\phi(t)$  denotes the phase of  $\langle \hat{\Delta}_0 \rangle_{\phi(t)}$ . For a linear phase change  $\phi(t) = \Omega_P t$  and upon performing the same response average which lead to Eq. (46) one therefore expects an amplitude response  $\langle \delta |\Delta_0| \rangle$  with a two-peak structure corresponding to the absorption and emission of a phase mode.

### III. GROUND-STATE PROPERTIES

We start with a consideration of our model’s ground-state properties. The technical details of the numerical minimization are briefly outlined in Appendix A.

We first consider the case without external CDW field  $\alpha_Q = 0$ . As well known,<sup>33</sup> a purely superconducting phase, i.e., with  $\eta_{co} = \delta\eta_{sc} = 0$  is stable for all  $U > 0$ . We display the resulting (real) order parameter  $\Delta_0$  in the superconducting ground state in Fig. 1 as a function of  $U/J$  for various band fillings. Note that, due to particle-hole symmetry, it is sufficient throughout this work to consider only results below half filling,  $n \equiv 2n_0 \leq 1$ .

Formally, a purely charge-ordered state can be induced from a second order instability above some critical value  $U_C$  that depends on the particle density  $n$ . An analytical



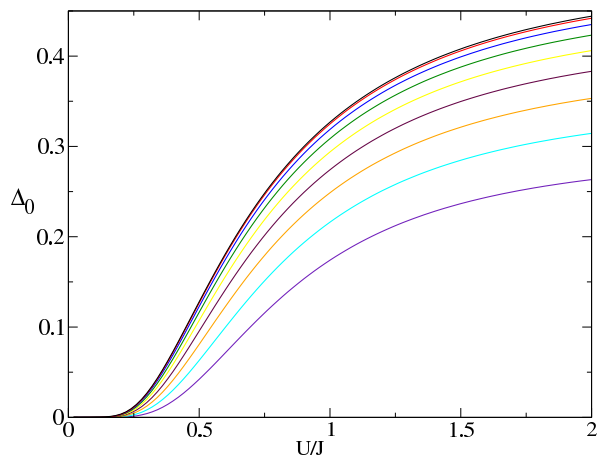


FIG. 1: Superconducting order parameter  $\Delta_0$  in the superconducting ground state as a function of  $U/J$  for band fillings  $n = 1, 0.9, 0.8, 0.7, 0.6, 0.5, 0.4, 0.3, 0.2$  (in descending order).

analysis of the energy functional reveals that  $U_C$  is given by

$$U_C = \left[ \int_{|\mu|}^J d\varepsilon \frac{D(\varepsilon)}{\varepsilon} \right]^{-1}, \quad (51)$$

which is displayed as a function of  $n$  in Fig. 2. At half filling, due to perfect nesting,  $U_C$  goes to zero and  $n = 1$  corresponds also to the peculiar situation where CDW and SC ground states are energetically degenerate. For all densities  $n$  away from half filling, the SC phase is lower in energy than the charge-ordered phase. This can be seen in Fig. 3 where we show the energy difference between the superconducting and the charge-ordered phase as a function of  $U/J$  for various values of  $n$ . The inset of this figure displays the corresponding charge or-

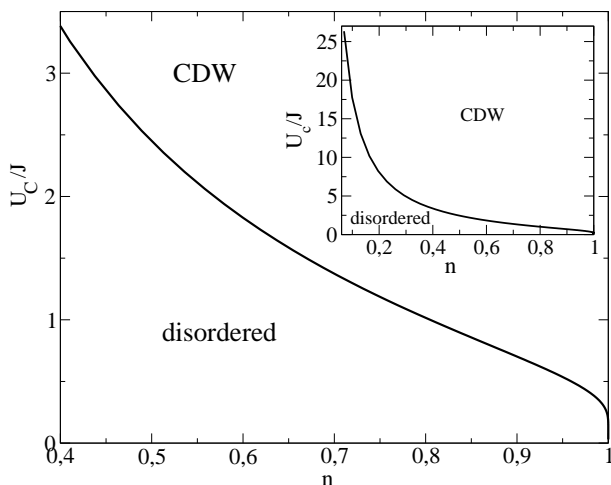


FIG. 2: Phase diagram for a pure charge-ordered phase (i.e., without SC) as a function of  $n$ ; Inset: the same result for a larger range of densities  $n$ .

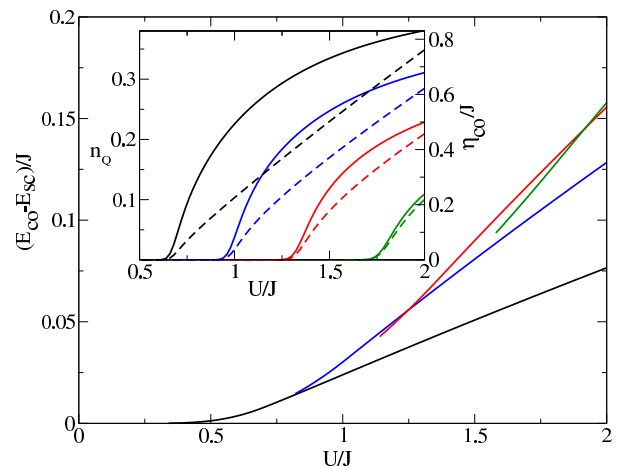


FIG. 3: Energy difference between the superconducting and the charge-ordered phase for  $n = 0.9$  (black),  $0.8$  (blue),  $0.7$  (red)  $0.6$  (green) as a function of  $U/J$ ; Inset: Corresponding results for the charge order parameter  $n_Q$  (solid lines) and the fields  $\eta_{co}$  (dashed lines)

der parameters  $n_Q$  and fields  $\eta_{co}$ . It should be mentioned that here we are restricted to a commensurate [i.e.,  $\mathbf{Q} = (\pi, \pi)$ ] CDW whereas away from half-filling incommensurate charge orders would be energetically more stable albeit still above the SC ground-state energy.

For Coulomb parameters of  $U$  where both phases are stable, it is conceivable that a coexistence phase, i.e., with  $\Delta_0$  and  $n_Q$  both non-zero, has an even lower energy. In our numerical analysis, however, we found such a phase to be always higher in energy than a pure superconducting one.

In order to stabilize charge order and to allow for situations with both order parameters finite, we introduce a non-zero charge-order field  $\alpha_Q$ , see Eq. 8. In its presence, a purely charge-ordered phase is obviously most favorable at half filling. Away from half filling, both order parameters  $n_Q$  and  $\Delta_0$  are non-zero in the ground state. We show the typical behavior of both parameters as a function of  $U$  for  $n = 1.0$  and  $n = 0.9$  in Fig. 4. The doping dependence of both quantities is displayed in Fig. 5. Note that in approaching half filling, the pairing order parameter is non-analytic,  $\Delta_0 \sim \sqrt{1-n}$ .

In the region  $U/J \lesssim 0.5$ , the superconducting order parameter shows a somewhat unexpected behavior because it gets larger when  $\alpha_Q$  is increased. In this regime the chemical potential falls in the range where the CDW opening induces a  $1/\sqrt{\omega}$  enhancement of the DOS. For larger  $U/J$  the SC order parameter gets suppressed by the CDW scattering as expected.

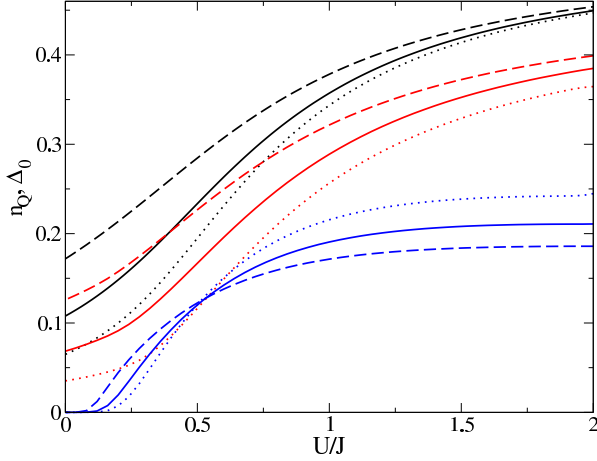


FIG. 4: Order parameters  $n_{\mathbf{Q}}$  (black ( $n = 1.0$ ) and red ( $n = 0.9$ )) and  $\Delta_0$  (blue ( $n = 0.9$ )) as a function of  $U/J$  for  $\alpha_{\mathbf{Q}} = 0.05, 0.1, 0.2$  (dotted, solid, dashed). Note that  $\Delta_0 = 0$  for  $n = 1.0$ .

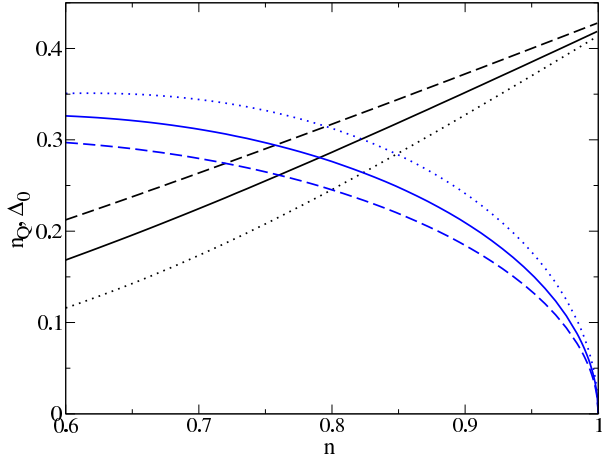


FIG. 5: Order parameters  $n_{\mathbf{Q}}$  (black) and  $\Delta_0$  (blue) as a function of charge concentration  $n$  for  $U/J = 1.5$  and  $\alpha_{\mathbf{Q}} = 0.05, 0.1, 0.2$  (dotted, solid, dashed)

#### IV. OUT-OF-EQUILIBRIUM DYNAMICS

In this chapter, we discuss the out-of-equilibrium dynamics of our model. In the first section, we consider situations without an external time-dependent perturbation (‘quantum-quench problems’), where the time dependence results from an initial state that is not the ground state. The problem of ‘pump and probe experiments’ is studied in the second section.

##### A. Quantum quench problems

We first consider the dynamics of our system that evolves from different initial density matrices. The latter are determined by the initial parameters  $\eta_{\text{sc}}^0, \eta_{\text{co}}^0, \delta\eta_{\text{sc}}^0$ .

In the following we shall always change these parameters relative to their ground state values,  $\eta_{\nu}^0 = \gamma\eta_{\nu}^{\text{gs}}$ . There are three different situations, (i) a purely charge-ordered phase ( $\eta_{\text{sc}}^0 = \delta\eta_{\text{sc}}^0 = 0$ ), (ii) a superconducting phase ( $\eta_{\text{co}}^0 = \delta\eta_{\text{sc}}^0 = 0$ ), and (iii) a coexistence phase of both orders where all  $\eta_{\nu}^{\text{gs}}$  are non-zero. Note that our dynamics does *not* evolve from a Hamiltonian with ‘quenched’ interaction parameters but only from a ‘quenched’ density matrix. This is different from previous studies<sup>27,28,43–47</sup> where in the context of the (repulsive) Hubbard model the local interaction  $U$  is set to a different value at  $t = 0$ .

We start with a consideration of case (i). In Fig. 6a we show  $n_{\mathbf{Q}}$  as a function of time  $t$  for  $U/J = 1.5$ ,  $n = 1.0$ ,  $\alpha_{\mathbf{Q}} = 0.2$  and several scaling factors  $\gamma$  between 0.05 and 3. The time-dependence of  $n_{\mathbf{Q}}$  has the generic structure expected for mean-field order parameters<sup>40</sup> which previously has been discussed in the context of SC<sup>34–37,39</sup> or antiferromagnetism.<sup>48</sup> This includes a  $\cos(2\eta_{\text{CO}}^{\infty}t)/\sqrt{\eta_{\text{CO}}^{\infty}t}$  relaxation of the amplitude towards a stationary value  $n_{\mathbf{Q}}^{\infty}$  which appears as a consequence of a ‘dephasing’ between the individual contributions of the scattering processes  $\mathbf{k} \rightarrow \mathbf{k} + \mathbf{Q}$  to the order parameter. Close to  $\gamma = 1$  the oscillatory frequency is determined by the amplitude excitations across the CDW gap  $2\eta_{\text{CO}}$ , which soften with increasing deviation from the equilibrium state towards a values  $\eta_{\text{CO}}^{\infty} = Un_{\mathbf{Q}}^{\infty} + \alpha_{\mathbf{Q}}/2$  for  $t \rightarrow \infty$ . The difference between this (reduced) stationary value as compared to the equilibrium result at  $\gamma = 1$  may be interpreted in terms of a population of excited HF states via an effective finite temperature  $T^{\text{eff}}$ . The latter is defined by the condition that the Fermi-Dirac distribution for  $T^{\text{eff}}$  leads to an equilibrium expectation value of  $\hat{n}_{\mathbf{Q}}$  that equals  $n_{\mathbf{Q}}^{\infty}$ . The values of these effective temperatures are given close to the corresponding curves in Fig. 6a.

The behavior of the dynamics changes for  $\gamma < 0.1$  where oscillations on much longer time scales emerge. In this regime one should go to very large times in order to obtain sensible results which conflicts with the stability of integration. We therefore abstain from an investigation of the extreme non-equilibrium regime.

The dependence of the CDW amplitude excitations on  $\gamma$ , obtained from the Fourier spectra of  $n_{\mathbf{Q}}(t)$ , is summarized in Fig. 6b. Close to  $\gamma = 1$  the linear-response dynamics of the CDW amplitude is described by a peak at  $\Omega = 2\eta_{\text{CO}}$  with small intensity (cf. spectra for  $\gamma = 0.9, 1.1$  in the insets) due to the strong mixing with quasiparticle excitations (indicated by the yellow shaded area). Upon increasing the non-equilibrium situation (i.e.,  $|\gamma - 1|$ ) the excitations soften and move inside the (equilibrium) CDW gap. Note that the equilibrium value of  $n_{\mathbf{Q}} \approx 0.43$  in Fig. 6 is close to the maximum value  $n_{\mathbf{Q}} = 0.5$  for a CDW at half-filling. Therefore one needs a large  $\gamma > 1$  in order to approximately obtain the same stationary value as for  $\gamma = 0.4$  and consequently also the CDW excitations are not symmetric with respect to  $\gamma = 1$ .

As an example for case (ii) we show in Fig. 7a the

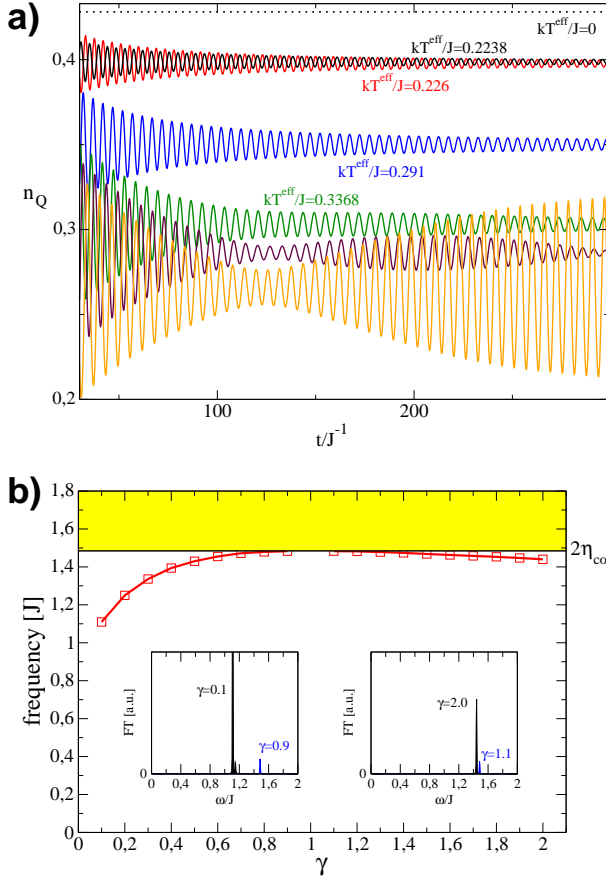


FIG. 6: a) Charge-order parameter  $n_Q$  as a function of time  $t$  for  $U/J = 1.5$ ,  $n = 1.0$ ,  $\alpha_Q = 0.2$ , and scaling factors  $\gamma = 3.0$  (black, solid),  $\gamma = 1.0$  (black, dotted),  $\gamma = 0.4$  (red),  $\gamma = 0.2$  (blue),  $\gamma = 0.1$  (green),  $\gamma = 0.075$  (maroon),  $\gamma = 0.05$  (orange). For moderate  $\gamma$  the envelope function can be fitted by  $n_Q^\infty \pm C/\sqrt{t}$  (dashed) and the effective temperature  $T^{\text{eff}}$ , as indicated in the lower panel, is defined as the temperature for which an equilibrium calculation yields  $n_Q^\infty$  for otherwise the same parameters. b) Frequency of the Fourier peaks as a function of  $\gamma$ . The insets detail the Fourier spectra for selected  $\gamma$  values. For  $\gamma \rightarrow 1$  the excitations approach the CDW gap  $2\eta_{CO}$ .

absolute value  $|\Delta_0|$  of the pairing order parameter as a function of time for  $U/J = 1.5$ ,  $n = 0.7$ , and several scaling factors  $\gamma$ . Similar to the previous case the time dependence is a damped oscillatory behavior  $\cos(2\eta_{SC}^\infty t)/\sqrt{\eta_{SC}^\infty t}$  which approaches  $\eta_{SC}^\infty$  for  $t \rightarrow \infty$ . The latter can again be described by an effective temperature  $T^{\text{eff}}$  as indicated adjacent to the corresponding curves.

Fig. 7b reports the time evolution of SC amplitude and phase for  $\gamma = 0.4$  together with their Fourier transforms. The gauge invariance of the TDHF approach implies conservation of charge which would be violated if one changes the order parameter in a BCS calculation without adjusting the chemical potential. Here charge conservation is obeyed in the non-equilibrium situation

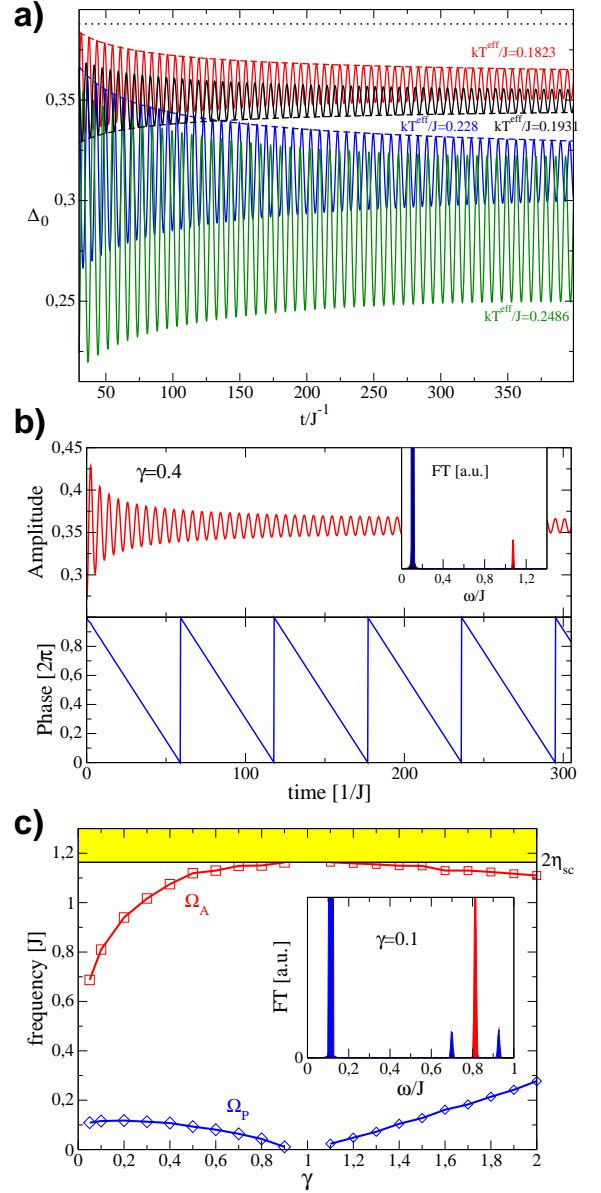


FIG. 7: a) Absolute value of the pairing order parameter  $|\Delta_0|$  as a function of time  $t$  for  $U/J = 1.5$ ,  $n = 0.7$ , and scaling factors  $\gamma = 3.0$  (black, solid),  $\gamma = 1.0$  (black, dotted),  $\gamma = 0.4$  (red),  $\gamma = 0.2$  (blue),  $\gamma = 0.125$  (green). Staggered CDW field  $\alpha_Q = 0$ . For moderate  $\gamma$  the envelope function can be fitted by  $n_Q^\infty \pm C/\sqrt{t}$  (dashed) and the effective temperature  $T^{\text{eff}}$ , as indicated adjacent to the curves, is defined as the temperature for which an equilibrium calculation yields  $n_Q^\infty$  for otherwise the same parameters. b) Time evolution of amplitude and phase for  $\gamma = 0.4$ . The inset shows the corresponding Fourier peaks of the main frequency (amplitude: red; phase: blue). c) Amplitude and phase excitation frequency as a function of the scaling parameter  $\gamma$ . The inset reports the Fourier spectrum for  $\gamma = 0.1$  demonstrating the coupling between amplitude and phase modes.

via the coupling to the phase mode which appears at a finite frequency  $\Omega_P$ . The dependence of both amplitude



excitation  $\Omega_A$  and phase mode  $\Omega_P$  on  $\gamma$  is summarized in Fig. 7c. The amplitude excitation for the SC order parameter has essentially the same behavior as for the charge order parameter in case (i) and develops from  $\Omega_A = 2\eta_{SC}$  at  $\gamma = 1$  inside the (equilibrium) SC gap upon decreasing or increasing  $\gamma$  from the equilibrium situation. In equilibrium the phase mode  $\Omega_P = 0$  reflecting its property as a Goldstone mode for the U(1) symmetry breaking. Upon deviating from equilibrium,  $\Omega_P$  moves inside the SC gap. The inset to Fig. 7c demonstrates the coupling between phase and amplitude excitation which reflects as two side peaks at  $\Omega_A \pm \Omega_P$  and which gets more pronounced upon increasing non-equilibrium. Note that such mixing is a common feature of superconductors in non-equilibrium and has recently also been exploited for two-band systems where a coupling between amplitude (Higgs) and Leggett modes can be induced.<sup>49</sup>

Finally, Fig. 8 reports the amplitude and phase dynamics for a ground state with both SC and CDW order and scaling factor  $\gamma = 0.6$ . A first obvious difference to the previous cases is that after a short transient response both SC and CDW order parameter oscillate with constant amplitude without any signature of relaxation. Second, the short period oscillation of CDW and SC amplitude is now clearly imprinted onto the phase dynamics which therefore reflects the strong coupling between amplitude and phase in this case. As a consequence and similar to the previous case, the phase mode now also appears in the form of side bands in the Fourier spectrum of the SC/CDW amplitude excitation which both appear at the same energy  $\Omega_A$ . Moreover, already at  $\gamma = 0.6$  higher-order excitations at  $2\Omega_A$  and  $2\Omega_A \pm \Omega_P$  are visible in the spectrum, though with rather small intensity. A more detailed inspection reveals also interference effects between phase and amplitude oscillations at  $\delta\omega = \Omega_A - 6\Omega_P$  which further split the phase excitations.

## B. Pump and probe simulations

Our general method of analyzing pump and probe situations has been described in Sec. II C. Depending on the values of  $\alpha_Q$  and  $n$  there can be three different equilibrium phases: a purely superconducting or charge-ordered phase, or a coexistence phases of both orders. We shall consider all three cases separately in the following sections. Since we can probe the response of the system to both, a pairing or a charge-order field there are six different setups in total that we need to consider.

### 1. Charge-order states

We first look at response functions in a charge-ordered phase as it is established in the ground state, e.g., for  $U/J = 1.5$ ,  $n = 1.0$ , and  $\alpha_Q = 0.2$ . The time dependence of  $n_Q$  in this case has been shown for several values of the initial scaling factor  $\gamma$  in Fig. 6a.

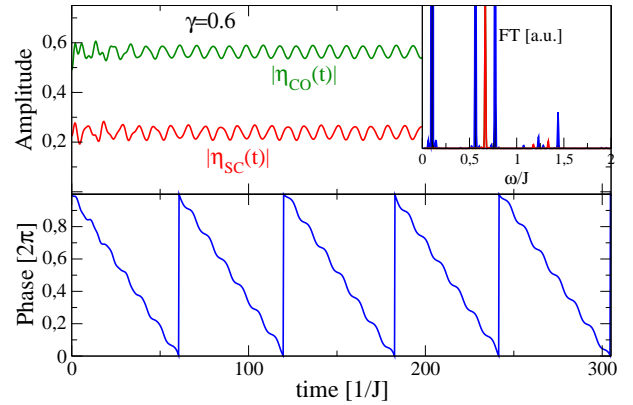


FIG. 8: Dynamics of CDW amplitude (green), SC amplitude (red) and SC phase (blue) for a system with both orders finite in the ground state. The inset reports the corresponding Fourier transforms (CDW and SC amplitude excitations occur at the same frequencies and therefore are undistinguishable). At  $t = 0$  the equilibrium values of the order parameters are scaled with  $\gamma = 0.6$ .  $U/t = 1.5$ ,  $\alpha_Q = 0.2$ ,  $n = 0.8$ .

We can probe the response of the system to both, a pairing or a charge-order field. Note that, without a probe pulse the pairing amplitude is zero. This means that for a pairing probe pulse, Eq. (49) simplifies to

$$\langle \delta|\Delta_0| \rangle = \frac{1}{\Delta t} \int_0^{\Delta t} dt |\langle \hat{\Delta}_0 \rangle_{\Phi_p(t)}|. \quad (52)$$

In Fig. 9 we show  $\langle \delta|\Delta_0| \rangle$ , as defined in (52), as a function of probe frequency for  $U/J = 1.5$ ,  $n = 1.0$ ,  $\alpha_Q = 0.2$  and several values of  $\gamma$ . The figure shows that the qualitative structure of the response does not change in the same range of  $\gamma$  values,  $3 \leq \gamma \leq 0.075$ , for which the quench dynamics [Fig. 6] shows the ‘regular’ damped oscillatory behavior. Starting from the equilibrium situation  $\gamma = 1$  one observes a shift of the response to higher frequencies upon increasing or decreasing  $\gamma$  without a change of the Lorentzian peak structure. This behavior is in qualitative agreement with the expectation from equilibrium linear-response theory (ELRT) which is derived for the present situation in appendix B and evaluated (dashed lines in Fig. 9) with the effective temperatures  $T^{\text{eff}}$ , introduced in Sec. IV A. Within this approximation, the pairing fluctuation, induced by the onsite-attraction  $U$ , generates poles within the CDW gap  $2\eta_{CO}$  (cf Fig. 15 in appendix B). Small values of  $U/J$  (compared to  $\eta_{CO}/J$ ) induce in-gap states close to the upper band edge  $2\eta_{CO}$  and with increasing fluctuation strength  $U/J$  the pole is shifted to lower energy inside the CDW gap.

As expected, for  $\gamma = 1$  ELRT agrees with the full TDHF result as can be seen from Fig. 9. A moderate non-equilibrium situation corresponds to an initial population of excited states and in ELRT can be modelled by a finite temperature for which the values are given in the lower panel of Fig. 6. One finds that upon increasing non-equilibrium, ELRT captures the reduction of peak

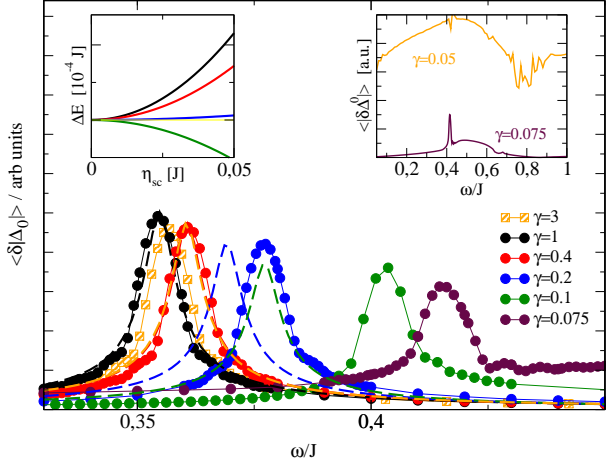


FIG. 9: Pairing response  $\langle \delta|\Delta_0| \rangle$  as a function of frequency  $\omega$  for  $U/J = 1.5$ ,  $n = 1.0$ ,  $\alpha_Q = 0.2$ , and scaling factors  $\gamma = 3.0$  (black, solid),  $\gamma = 1.0$  (black, dotted),  $\gamma = 0.4$  (red),  $\gamma = 0.2$  (blue),  $\gamma = 0.1$  (green),  $\gamma = 0.075$  (maroon). ELRT results are shown with dashed lines and are obtained for the effective temperatures indicated in the lower panel of Fig. 6. Upper right inset: Same quantities for  $\gamma = 0.075$  (maroon),  $\gamma = 0.05$  (orange). Upper left inset: Change  $\Delta E \equiv E(\eta_{sc}) - E(\eta_{sc} = 0)$  of the energy as a function of  $\eta_{sc}/J$  for stationary states with  $U/J = 1.5$ ,  $n = 1.0$ ,  $\alpha_Q = 0.2$ , and expectation values  $n_Q \approx 0.43$  (black),  $n_Q = 0.4$  (red),  $n_Q = 0.35$  (blue),  $n_Q = 0.3$  (green).

intensity and the shift of the peak to higher energy, however, it under(over)estimates the latter upon decreasing (increasing)  $\gamma$  from  $\gamma = 1$ .

Only for values of  $\gamma$  below 0.075, the linear-response assumption seems to break down almost instantaneously, see the inset of Fig. 9, where also the quench dynamics changes.

In an equilibrium situation the collective excitation frequency  $\Omega$  of an observable  $\mathcal{O}$  can be deduced from the curvature of the energy functional around the saddle point, i.e.,  $\Omega^2 \sim \partial^2 E / \partial (\delta\mathcal{O})^2$ . In this spirit one could argue that the hardening of the excitation in Fig. (9) is due to a stiffening of the ground state energy functional as a function of the dynamical variable, in our case  $\Delta_0$ . Such an interpretation, however, fails in our out-of-equilibrium situation. This is illustrated in the upper left inset to Fig. 9 where we show the energy change as a function of  $\eta_{sc}$  that is induced in a stationary state for values of  $n_Q$  that equal those in the long time for  $\gamma = 3.0, 0.4, 0.2, 0.1$ , see Fig. 6a. As one may expect, by shifting the system away from its ground state, pairing becomes energetically less costly and for  $n_Q \lesssim 0.3$  it even lowers the energy. Hence, the stiffness argument would predict a softening rather than a hardening of the excitations as shown in the main panel of Fig. 9.

One must keep in mind that, while the expectation values of  $\hat{n}_Q$  and consequently of  $\hat{H}_0$  become stationary in the long time limit, the density matrix does not. Therefore, the stationary states considered in the left up-

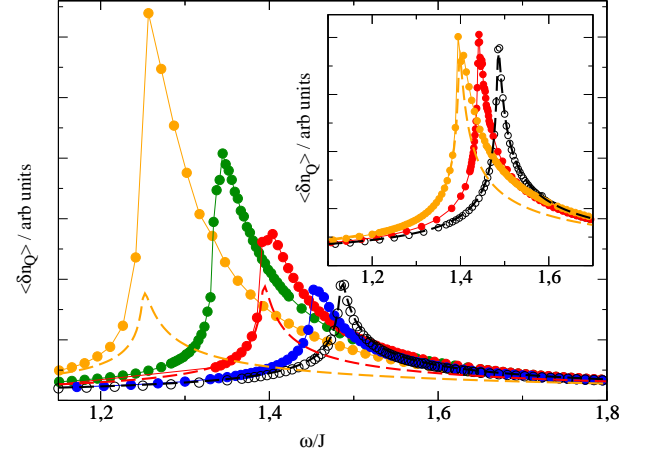


FIG. 10: Charge-order response  $\langle \delta n_Q \rangle$  as a function of frequency  $\omega$  for  $U/J = 1.5$ ,  $n = 1.0$ ,  $\alpha_Q = 0.2$ , and scaling factors  $\gamma = 1.0$  (black, dotted),  $\gamma = 0.6$  (blue),  $\gamma = 0.4$  (red),  $\gamma = 0.3$  (green),  $\gamma = 0.2$  (orange). Inset: Same quantities for  $\gamma = 1.0$  (black, dotted),  $\gamma = 1.5$  (blue),  $\gamma = 2.0$  (red),  $\gamma = 2.5$  (green),  $\gamma = 3.0$  (orange). ELRT results are shown with dashed lines and are obtained for the effective temperatures indicated in the lower panel of Fig. 6.

per inset to Fig. 9 have not much in common with the time-dependent long time states in Fig. 6, apart from the expectation value of  $\hat{n}_Q$ . It is therefore interesting to observe that in an out-of-equilibrium situation the long-time limits of  $\hat{n}_Q$  yield the qualitatively correct behavior of the peak shifts in an effective temperature ELRT while the analysis of the stiffness in the energy functional fails.

A charge-order probe pulse obviously detects the amplitude excitation as shown in Fig. 6c. This implies not only a shift of the peak position to lower energies but also a significant increase of its weight. As already mentioned in the previous section the stark asymmetry in the spectra with respect to  $\gamma = 1$  is due to the fact that the underlying equilibrium CDW order parameter  $\eta_{CO}$  is close to its fully polarized value.

We can also try to understand the peak positions from the ELRT analysis (cf. appendix B). Without staggered field ( $\alpha_Q = 0$ ) the collective CDW excitation appears at the frequency of the CDW gap  $\omega = 2\eta_{CO}$ . A finite  $\alpha_Q$  pushes this excitation into the quasiparticle continuum, however, the intensity of the RPA response function  $\chi^{\text{cdw}}(\omega) = \chi_0^{\text{cdw}}(\omega)/(1 - V_Q\chi_0^{\text{cdw}}(\omega))$  is still maximum at the CDW gap frequency due to (a) the enhancement of the bare correlations  $\chi_0^{\text{cdw}}(\omega)$  and (b) the minimum of  $\Re[1 - V_Q\chi_0^{\text{cdw}}(\omega)]$  at  $\omega = 2\eta_{CO}$ . In fact, the peaks in the TDHF results shown in Fig. 10 occur exactly at the values  $\omega = 2\eta^\infty = |U|n_Q^\infty + \alpha_Q/2$  with  $n_Q^\infty$  being the long-time stationary value (cf. Fig. 6a) from which we have defined the effective temperatures and for which the ELRT results are shown with the dashed curves in Fig. 10. Thus, while the peak positions between TDHF and effective temperature ELRT show very good agreement, the intensities strongly deviate in particular for

$\gamma < 1$  where the response in TDHF gets strongly enhanced.

At first sight, one might think that this enhancement of spectral weight is a natural behavior that simply results from the larger amplitudes of the underlying out-of-equilibrium oscillations in Fig. 6a. In fact, as we show in Appendix C, the very same behavior is found in the rather simple model of a one-dimensional classical oscillator. It is crucial, however, to include an anharmonic term into the potential of that model. Without it, i.e., for a linear equation of motion, no weight gain is observed. We also do not find such a weight gain, when we calculate the exact out-of-equilibrium response function for a two-site (negative  $U$ ) Hubbard model, see Appendix D. This is not surprising because here, as well, we solve a set of 4 *linear* differential equations with constant coefficients. In contrast, the TDHF equations for the same model are non-linear. For this reason, we do observe a weight gain which, at least for the two-site model, is clearly a spurious result. We can therefore not rule out the possibility that the weight-gain observations in the infinite model that we presented in this section are artifacts of an oversimplifying TDHF method. In contrast, our previous observation that position and weight of the pairing response function are rather robust when we go away from equilibrium is confirmed by the exact results for the two-site Hubbard model in Appendix D.

## 2. Superconducting ground state

Next we consider the case with  $U/J = 1.5$ ,  $n = 0.7$ ,  $\alpha_Q = 0$  where the system has a pure superconducting ground state.

We start our discussion with the pairing response function which is shown in Fig. 11 for scaling factors  $\gamma$  between 0.125 and 3 for which the corresponding amplitude and phase excitations have been reported in Fig. 7c.

In the equilibrium limit ( $\gamma = 1$ ) the TDHF response is perfectly reproduced by ELRT (dashed) which describes the amplitude excitation (or ‘Higgs mode’) at twice the superconducting gap. Upon increasing the non-equilibrium situation (i.e., deviating from  $\gamma = 1$ ) one observes two main features beyond the ELRT expectation: first, the amplitude excitation splits into two peaks and second, additional weight is observed at low energies. In fact, applying the effective temperature ELRT yields a single peak located between the excitations of the TDHF result (cf. result for  $\gamma = 0.4$  in the upper panel of Fig. 11). The reason for the splitting of the amplitude excitation has been discussed in Sec. IIC and is related to the definition of the pairing response function Eq. (49) which for the present situation is influenced by the phase mode of the underlying non-equilibrium state (cf. Fig. 7c.) Therefore the response  $\langle |\delta\Delta_0| \rangle$  is determined by excitations appearing at frequencies  $\Omega_A \pm \Omega_P$ , where  $\Omega_{A,P}$  correspond to amplitude and phase modes, respectively. The lower panel of Fig. 11 demonstrates the

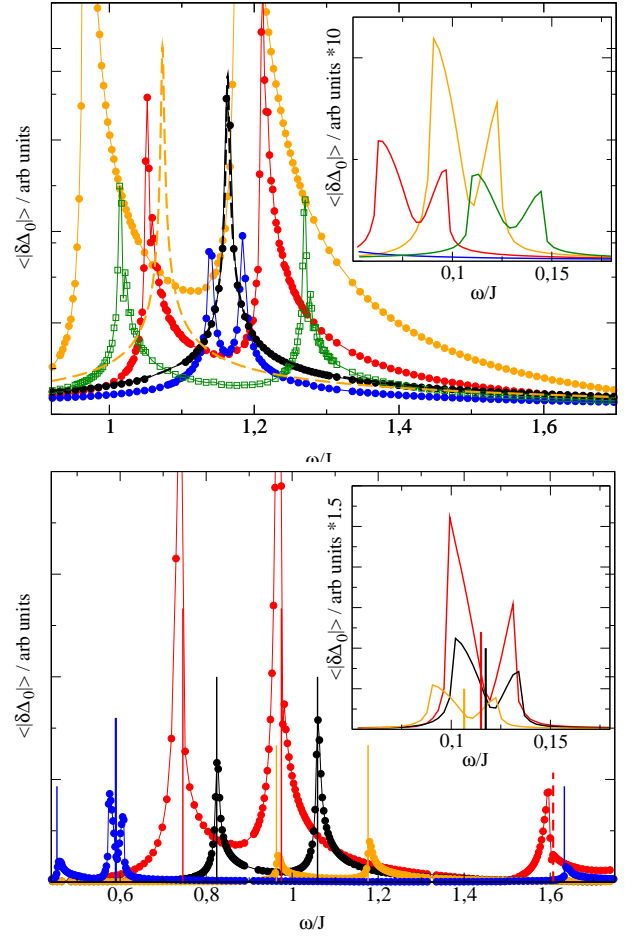


FIG. 11: Pairing response  $\langle |\delta\Delta_0| \rangle$  as a function of frequency  $\omega$  for  $U/J = 1.5$ ,  $n = 0.7$ ,  $\alpha_Q = 0$ . Top: scaling factors  $\gamma = 1.0$  (black, dotted),  $\gamma = 0.9$  (blue),  $\gamma = 0.6$  (red),  $\gamma = 0.4$  (orange),  $\gamma = 1.5$  (green). Inset: same quantities for a smaller frequency range. Bottom: scaling factors  $\gamma = 0.4$  (orange),  $\gamma = 0.2$  (black),  $\gamma = 0.125$  (red),  $\gamma = 3.0$  (blue). Inset: same quantities for a smaller frequency range. The vertical thin lines correspond to energies  $\Omega_A \pm \Omega_P$  as deduced from the Fourier transform of amplitude and phase modes (cf. Fig. 7). The thick lines are phase modes whereas the red dashed vertical line is an excitation at  $2\Omega_A - \Omega_P$  for  $\gamma = 0.125$ .

consistency of our analysis for various  $\gamma$  values.

In contrast, the effective temperature ELRT only yields a renormalized (softened) amplitude mode and thus cannot account for the splitting when the response is evaluated within Eq. (46). Also an evaluation based on Eq. (44) does not yield a splitting since the phase mode in ELRT always occurs at  $\Omega_P = 0$ .

Moreover, for strong non-equilibrium initial states one observes further non-linear processes as the appearance of an excitation at  $2\Omega_A - \Omega_P$  for  $\gamma = 0.125$ . As mentioned above the second feature concerns the low energy spectral weight as shown in the insets to Fig. 11 which can also be attributed to the coupling between phase and amplitude degrees of freedom at strong non-equilibrium. These low energy excitations are also split by  $\omega_P \pm g^2/\Omega_A$

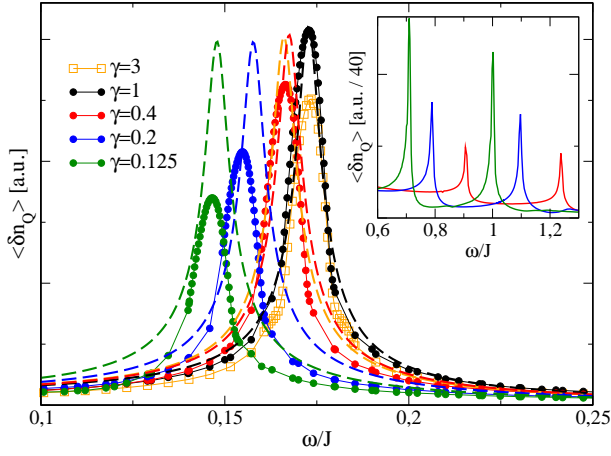


FIG. 12: Charge-order response  $\langle \delta n_{\mathbf{Q}} \rangle$  as a function of frequency  $\omega$  for  $U/J = 1.5$ ,  $n = 0.7$ ,  $\alpha_{\mathbf{Q}} = 0$ , and scaling factors  $\gamma = 3.0$  (black, solid),  $\gamma = 1.0$  (black, dotted),  $\gamma = 0.4$  (red),  $\gamma = 0.2$  (blue),  $\gamma = 0.125$  (green): Inset: Same quantities at larger frequencies.

where  $g$  denotes an effective coupling parameter between amplitude and phase.

We proceed with the analysis of the charge-order response which is shown in Fig. 12 again for various initial non-equilibrium situations parametrized by  $\gamma$ . At half-filling the charge response at  $\mathbf{q} = \mathbf{Q}$  would occur at zero frequency due to the degeneracy between CDW and SC. Finite doping shifts this excitation to finite frequency inside the SC gap (cf. Fig. 1 in Ref. [50]) and Fig. 12 reveals that in the equilibrium situation ( $\gamma = 1$ ) our TDHF response is perfectly described by ELRT (dashed). For stronger non-equilibrium situations the effective temperature ELRT still gives a reasonable description of the mode softening but does not capture the reduction in intensity of the TDHF charge-order response. Moreover, in non-equilibrium the charge order excitations at  $\mathbf{q} = \mathbf{Q}$  can couple to the pairing modes at  $\mathbf{q} = 0$  (cf. Fig. 11 which induces the high energy features shown in the inset to Fig. 12. Note that in this case the splitting is not exactly  $2\Omega_P$  but also influenced by the coupling strength between charge and pairing modes.

### 3. Ground state with finite pairing and charge order parameters

Finally, as an example for a coexistence phase we consider the case where  $U/J = 1.5$ ,  $n = 0.8$ ,  $\alpha_{\mathbf{Q}} = 0.2$ . For these parameters,  $\Delta_0$  and  $n_{\mathbf{Q}}$  have approximately the same values (cf. Fig. 4) and none of the two orders dominates.

In Fig. 13 we show the pairing response in the equilibrium ( $\gamma = 1$ ) and non-equilibrium situation ( $\gamma \neq 0$ ). The linear-response for a coupled CDW-SC system has been recently analyzed in Ref. 41 in the context of the visibility of the amplitude ('Higgs') mode within linear

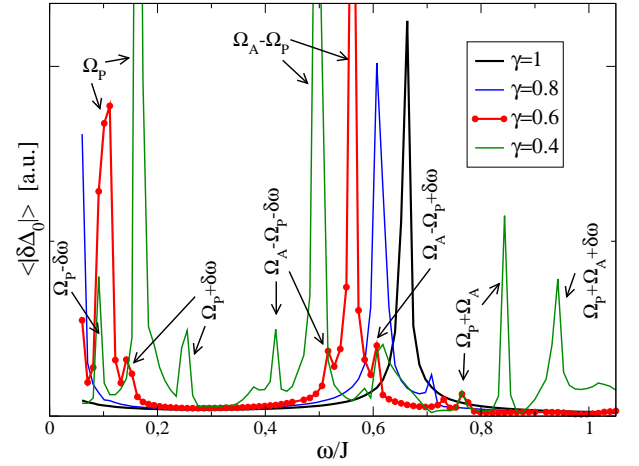


FIG. 13: Pairing response  $\langle \delta |\Delta_0| \rangle$  as a function of frequency  $\omega$  for  $U/J = 1.5$ ,  $n = 0.8$ ,  $\alpha_{\mathbf{Q}} = 0.2$  and scaling factors  $\gamma = 1.0$  (black, dotted),  $\gamma = 0.8$  (blue),  $\gamma = 0.6$  (red),  $\gamma = 0.4$  (green). Coupled amplitude and phase excitations as deduced from Fig. 8 are indicated for the  $\gamma = 0.4, 0.6$  results.

(Raman) response.<sup>41</sup> In fact, the presence of CDW order pushes the linear response amplitude excitation to  $\Omega_A \approx 0.66J$ , i.e. well below the  $-E_-(\mathbf{k}_F) \rightarrow +E_-(\mathbf{k}_F) \approx 1.2J$  transition [cf. Eq. (28)] where it would appear in the pure SC case. In the non-equilibrium case the individual peaks can be understood from an inspection of the corresponding time evolution of the order parameters as shown in Fig. 8 for the case  $\gamma = 0.6$  and from the general structure of the pairing response function as given in Eq. (44). The latter couples the phase to the amplitude modes, similar to what is already observed in the bare SC case Fig. 11, yielding excitations at  $\Omega_A \pm \Omega_P$  plus the phase mode at  $\Omega_P$ . An additional feature concerns the interference effect between phase and amplitude excitation which occurs at

$$\delta\omega = \Omega_A - 6\Omega_P \quad (53)$$

and generates further satellite peaks to the main excitations discussed above.

Since we consider a commensurate charge order at  $\mathbf{Q} = (\pi, \pi)$  the corresponding order parameter can always be chosen as real and there is no associated phase degree of freedom. Thus the charge order response, as shown in Fig. 14 occurs at  $\Omega_A$ . Note, however, that the charge and SC amplitudes are coupled which induces the satellite peaks at  $\Omega_A \pm \delta\omega$ . Increasing the non-equilibrium situation to  $\gamma = 0.4$  induces further satellites related to phase modes and their coupling to the amplitude excitations. In any case, it is obvious that in the non-equilibrium situation both, charge and pairing response cannot be captured by ELRT which does not account neither for the coupling of amplitude and phase nor the satellite structure due to the interference scale  $\delta\omega$ .



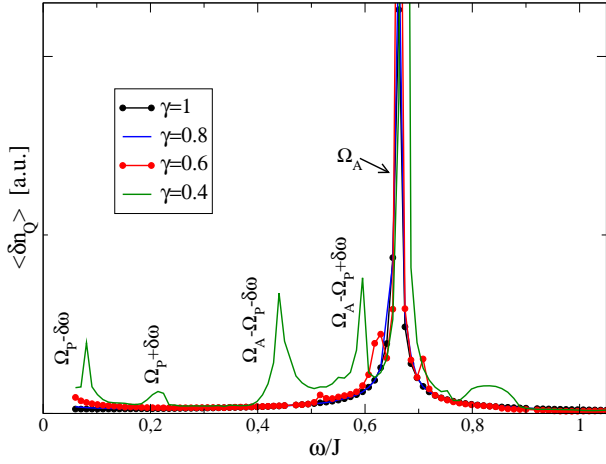


FIG. 14: Charge order response  $\langle \delta n_{\mathbf{Q}} \rangle$  as a function of frequency  $\omega$  for  $U/J = 1.5$ ,  $n = 0.8$ ,  $\alpha_{\mathbf{Q}} = 0.2$  and scaling factors  $\gamma = 1.0$  (black, dotted),  $\gamma = 0.8$  (blue),  $\gamma = 0.6$  (red),  $\gamma = 0.4$  (green). Coupled amplitude and phase excitations as deduced from Fig. 8 are indicated for the  $\gamma = 0.4, 0.6$  results.

## V. CONCLUSIONS

In this work, we have investigated pairing and charge-order response functions in out-of-equilibrium states of the negative  $U$  Hubbard model by means of the time-dependent Hartree-Fock approximation (TDHF). In particular, we have focussed on the coupling between amplitude and phase excitations which can be inherent in the definition of the response function [cf. Eq. (50)] but also be induced in a non-equilibrium situation.

We have allowed for an additional charge-order field in the Hamiltonian which simulates the effect of a lattice modulation. In this way, our model can have three types of ground states, a pure superconducting state, a charge-order state, or a state with both orders present. A pump-pulse may then drive the system into non-equilibrium states of the same symmetry.

Since the TDHF can be applied in all non-equilibrium situations, we did not have to rely on any linear-response assumptions that are inherent, e.g., in the Kubo formula. In this way our study also revealed, if and under what circumstances such an assumption is justified in non-equilibrium calculations. It turned out that a linear-response assumption, based on an effective temperature description of the underlying non-equilibrium state, qualitatively accounts for the spectra when the latter is due to a pure CDW dynamics without any coupling to phase degrees of freedom. In these cases (Figs. 9 and 10) ELRT works for not too large deviations from  $\gamma = 1$  but fails to reproduce the excitation energy or (and) peak intensity in stronger non-equilibrium situations. For an underlying non-equilibrium SC state the appearance of a finite frequency phase mode has significant consequences for the pairing and charge order response. Concerning the latter, ELRT correctly describes the formation of in-gap

excitations (cf. Fig. 12), although underestimating the intensity, while it fails to describe the amplitude-phase coupling in strong non-equilibrium which induces the appearance of split peaks on the scale of the SC gap. The same holds in case of the pairing response where the splitting is due to the appearance of the phase mode in the definition of the response Eq. (50) and when the non-equilibrium state is an admixture of both, CDW and SC.

In this work, we have considered a neutral system without long-range Coulomb interactions which due to the Anderson-Higgs mechanism<sup>51</sup> would push the phase mode up to the plasma frequency. For a two-dimensional system the plasma frequency would be still at low energy  $\omega_p \sim \sqrt{|\mathbf{q}|}$  so that for these systems our results could be still meaningful. Also disorder helps to push the plasma frequency to lower energies due to the reduced superfluid density.

The interplay of CDW and SC in the attractive Hubbard model has been investigated previously<sup>41</sup> in the context of the visibility of the amplitude (‘Higgs’) mode in charge-density wave superconductors such as NbSe<sub>2</sub>. These authors were interested in the Raman response which amounts to the evaluation of the charge response function at momentum  $\mathbf{q} = 0$ . Here, instead we have studied the charge response function at the momentum of the CDW  $\mathbf{q} = \mathbf{Q}$  which in principle can be measured with inelastic x-ray scattering or indirectly with neutrons via the coupling to the lattice. The pairing response can be experimentally accessed with the Josephson effect which has been previously used to investigate the contribution of pair fluctuations to the pseudogap formation in high- $T_c$  superconductors.<sup>52</sup>

While the measurement of these responses for CDW superconductors would be definitely interesting to compare with our predictions, an equally important issue of the present paper concerns the validity of linear-response theory in a non-equilibrium situation with regard to pump-probe experiments. Methodologically our investigations are based on the TDHF approximation which can be viewed as the simplest approach to study the dynamics of interacting systems and therefore one has to be aware of its limitations. In this regard, one aspect concerns the damping of the order parameter which in TDHF is caused by a ‘dephasing’ of oscillations for the different Hartree Fock single-particle energies. Genuine many-particle relaxation processes are not covered by the TDHF and it is therefore bound to become inaccurate in the limit  $t \gg J^{-1}$ . In pump-and-probe experiments, however, the probe pulse is usually applied in a time period where the excitation induced by the pump pulse is still far from relaxation. Hence, we are confident, that the TDHF constitutes a meaningful first-order approximation to these problems.

We have also critically examined our observations by looking into two simple toy models. Our findings seem to be confirmed when we consider a simple anharmonic classical oscillator. Due to the non-linear term in the equation of motion, the response to a small external field



also depends strongly on the amplitude of the underlying oscillation. In contrast, however, the exact solution for the charge-order response of a two-site Hubbard model is, in this regard, different from what the TDHF method finds. The reason for this difference is the non-linearity that the TDHF spuriously introduces into its equations of motion. It remains an open question, if these deficiencies of the TDHF are a generic problem of that method or can be explained by the particular nature of the low-dimensional two-site Hubbard model.

For the negative  $U$  Hubbard model, there are more sophisticated methods available that could be used to study the out-of-equilibrium response functions which we have investigated in this work. The most obvious way to improve the TDHF is to use Gutzwiller wave functions instead of single-particle product wave functions.<sup>27–29,53–57</sup> Work in this direction is in progress. Other conceivable approaches are the out-of-equilibrium DMFT or purely numerical methods such as DMRG, quantum Monte-Carlo, or exact diagonalization. Our TDHF results constitute a useful first-order approximation in all such future investigations.

### Acknowledgements

This work was supported by the Deutsche Forschungsgemeinschaft (DFG) under SE 806/18-1.

### Appendix A: Minimisation algorithm

For the numerical minimization of our energy functional, we need to solve the equation

$$[\tilde{h}_{\varepsilon_i}, \tilde{\rho}_{\varepsilon_i}] = 0 \quad (\text{A1})$$

self-consistently for all energies  $\varepsilon_i$  and obeying the additional constraint  $\tilde{\rho}_{\varepsilon_i}^2 = \tilde{\rho}_{\varepsilon_i}$  for single-particle wave functions. This equation is readily solved numerically by determining the eigenvectors and eigenvalues of  $\tilde{h}_{\varepsilon_i}$ . We have determined the minimum with the following algorithm

- i) We start with some small, but non-zero, (input) values for the fields  $\eta_{\text{sc}}^i, \eta_{\text{co}}^i, \delta\eta_{\text{sc}}^i$  and set up the matrices  $\tilde{h}_{\varepsilon_i}$  for each of the  $N_{\text{disk}}$  energies  $\varepsilon_i$ .
- ii) For each  $\varepsilon_i$ , we solve Eq. (A1).
- iii) With  $\tilde{\rho}_{\varepsilon_i}$ , new values  $\eta_{\text{sc}}^o, \eta_{\text{co}}^o, \delta\eta_{\text{sc}}^o$  are determined using (11)-(13) and (29)-(31). With these values, we could go back to i). However, it is usually necessary to introduce some ‘damping factor’  $\beta < 1$  and continue with, e.g.,  $\eta_{\text{sc}}^i \rightarrow \eta_{\text{sc}}^i + \beta(\eta_{\text{sc}}^o - \eta_{\text{sc}}^i)$ . Without such a damping, it is not ensured that the energy decreases in each step of our algorithm.
- iv) The algorithm terminates when the fields in iii) are approximately the same as the input values in i).

### Appendix B: Equilibrium linear-response theory (ELRT) for a SC perturbation of a CDW ground state

The Hamiltonian for a CDW is given by

$$H = \sum_{\mathbf{k}, \sigma} (\varepsilon_{\mathbf{k}} - \mu) \hat{c}_{\mathbf{k}, \sigma}^\dagger \hat{c}_{\mathbf{k}, \sigma} + \eta \sum_{\mathbf{k}, \sigma} (\varepsilon_{\mathbf{k}} - \mu) \hat{c}_{\mathbf{k}+\mathbf{Q}, \sigma}^\dagger \hat{c}_{\mathbf{k}, \sigma} \quad (\text{B1})$$

with  $\mathbf{Q} = (\pi, \pi)$  and  $\varepsilon_{\mathbf{k}} = -\varepsilon_{\mathbf{k}+\mathbf{Q}}$ . The transformation

$$\begin{aligned} \hat{c}_{\mathbf{k}, \sigma} &= \beta_{\mathbf{k}} \hat{a}_{\mathbf{k}, -\sigma} + \alpha_{\mathbf{k}} \hat{a}_{\mathbf{k}, +\sigma}, \\ \hat{c}_{\mathbf{k}+\mathbf{Q}, \sigma} &= -\alpha_{\mathbf{k}} \hat{a}_{\mathbf{k}, -\sigma} + \beta_{\mathbf{k}} \hat{a}_{\mathbf{k}, +\sigma} \end{aligned}$$

diagonalizes Eq. (B1) and yields

$$H = \sum_{\mathbf{k} \in \mathcal{B}_0, \sigma} \left[ (-\mu + E_{\mathbf{k}}^+) \hat{a}_{\mathbf{k}, +\sigma}^\dagger \hat{a}_{\mathbf{k}, +\sigma} + (-\mu + E_{\mathbf{k}}^-) \hat{a}_{\mathbf{k}, -\sigma}^\dagger \hat{a}_{\mathbf{k}, -\sigma} \right] \quad (\text{B2})$$

with

$$\begin{aligned} \alpha_{\mathbf{k}} &= \frac{1}{\sqrt{2}} \sqrt{1 + \frac{\varepsilon_{\mathbf{k}}}{E_{\mathbf{k}}}}, \\ \beta_{\mathbf{k}} &= \frac{1}{\sqrt{2}} \sqrt{1 - \frac{\varepsilon_{\mathbf{k}}}{E_{\mathbf{k}}}} \end{aligned}$$

where  $E_{\mathbf{k}}^\pm = \pm \sqrt{\varepsilon_{\mathbf{k}}^2 + \Delta^2}$  and  $\mathcal{B}_0$  is the reduced Brillouin zone introduced in Sec. II A.

#### 1. Pair fluctuations

We use the pairing operators  $\hat{\Delta}_0$  and  $\hat{\Delta}_{\mathbf{Q}}$ , as introduced in (11) and (12) to define the corresponding pair correlation functions

$$\begin{aligned} \chi_0^{\Delta_0^\dagger \Delta_0} &= -i \langle \mathcal{T} \hat{\Delta}_0^\dagger \hat{\Delta}_0 \rangle, \\ \chi_0^{\Delta_{\mathbf{Q}}^\dagger \Delta_{\mathbf{Q}}} &= -i \langle \mathcal{T} \hat{\Delta}_{\mathbf{Q}}^\dagger \hat{\Delta}_{\mathbf{Q}} \rangle, \\ \chi_0^{\Delta_0^\dagger \Delta_{\mathbf{Q}}} &= -i \langle \mathcal{T} \hat{\Delta}_0^\dagger \hat{\Delta}_{\mathbf{Q}} \rangle, \\ \chi_0^{\Delta_{\mathbf{Q}}^\dagger \Delta_0} &= -i \langle \mathcal{T} \hat{\Delta}_{\mathbf{Q}}^\dagger \hat{\Delta}_0 \rangle. \end{aligned}$$

One obtains

$$\begin{aligned} \chi_0^{\Delta_0^\dagger \Delta_0}(\omega) &= -\frac{1}{N} \sum_{\mathbf{k} \in \mathcal{B}_0, s=\pm} \frac{1 - 2f(E_{\mathbf{k}}^s - \mu)}{\omega - 2\mu + 2E_{\mathbf{k}}^s}, \\ \chi_0^{\Delta_{\mathbf{Q}}^\dagger \Delta_{\mathbf{Q}}}(\omega) &= -\frac{1}{N} \sum_{\mathbf{k}, s=\pm} \frac{\eta^2}{E_{\mathbf{k}}^2} \frac{1 - 2f(E_{\mathbf{k}}^s - \mu)}{\omega - 2\mu + 2E_{\mathbf{k}}^s}, \\ &\quad -\frac{1}{N} \sum_{\mathbf{k} \in \mathcal{B}_0, s=\pm} \frac{\varepsilon_{\mathbf{k}}^2}{E_{\mathbf{k}}^2} \frac{1 - f(E_{\mathbf{k}}^+ - \mu) - f(E_{\mathbf{k}}^- - \mu)}{\omega - 2\mu}, \\ \chi_0^{\Delta_0^\dagger \Delta_{\mathbf{Q}}}(\omega) &= \chi_0^{\Delta_{\mathbf{Q}}^\dagger \Delta_0}(\omega), \\ &= -\frac{1}{N} \sum_{\mathbf{k} \in \mathcal{B}_0, s=\pm} s \frac{\eta}{E_{\mathbf{k}}} \frac{1 - 2f(E_{\mathbf{k}}^s - \mu)}{\omega - 2\mu + 2E_{\mathbf{k}}^s}, \end{aligned}$$

## 2. CDW fluctuations

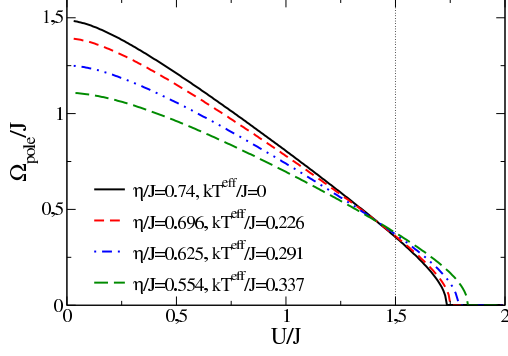


FIG. 15: Poles  $\Omega_{\text{pole}}$  within the CDW gap  $2\eta$  induced by a SC perturbation Eq. (B3) at half-filling and for the temperatures for which the ELRT results are shown in Fig. 9.

which we evaluate with the density of states  $D(\varepsilon)$  as defined in Eq. (34).

We now consider a perturbation from pairing fluctuations as, e.g., arising from an attractive on-site interaction

$$\hat{V} = -\frac{|U|}{N} \sum_{\mathbf{q}} \hat{\Delta}_{\mathbf{q}}^{\dagger} \hat{\Delta}_{\mathbf{q}} \quad (\text{B3})$$

with

$$\hat{\Delta}_{\mathbf{q}} \equiv \frac{1}{L} \sum_{\mathbf{k}} \hat{c}_{\mathbf{k},\uparrow}^{\dagger} \hat{c}_{-\mathbf{k}-\mathbf{q},\downarrow}^{\dagger}, \quad (\text{B4})$$

which yields the following RPA problem for the pair correlation functions

$$\underline{\underline{\chi}} = \underline{\underline{\chi}}_0 + \underline{\underline{\chi}}_0 \underline{\underline{V}} \underline{\underline{\chi}} \quad (\text{B5})$$

with

$$\underline{\underline{\chi}}_0 = \begin{pmatrix} \Delta_0^{\dagger} \Delta_0 & \Delta_0^{\dagger} \Delta_{\mathbf{Q}} \\ \chi_0^{\Delta_0^{\dagger} \Delta_0} & \chi_0^{\Delta_0^{\dagger} \Delta_{\mathbf{Q}}} \\ \chi_0^{\Delta_{\mathbf{Q}}^{\dagger} \Delta_0} & \chi_0^{\Delta_{\mathbf{Q}}^{\dagger} \Delta_{\mathbf{Q}}} \end{pmatrix} \quad (\text{B6})$$

and

$$\underline{\underline{V}} = \begin{pmatrix} -|U| & 0 \\ 0 & -|U| \end{pmatrix}. \quad (\text{B7})$$

The poles  $\Omega_{\text{pole}}$  within the CDW gap  $2\eta$  can then be determined from the condition

$$\text{DET}[\underline{\underline{1}} - \underline{\underline{\chi}}_0 \underline{\underline{V}}] = 0 \quad (\text{B8})$$

which for  $\omega = 0$  corresponds to the standard Thouless criterion for a SC instability. The solutions of Eq. (B8) are shown in Fig. 15 and with increasing  $U/J$  move from the CDW gap at  $\Omega_{\text{pole}} = 2\eta_{CO}$  to  $\Omega_{\text{pole}} = 0$  where the SC instability is reached. Note, however, that the curves in Fig. 15 are obtained for *fixed*  $\eta$  whereas in the present HF theory  $\eta_{CO}$  itself is an increasing function of  $|U|$  so that the instability is never reached at half-filling.

The (Hermitian) operator  $\hat{n}_{\mathbf{Q}}$  for CDW fluctuations has been defined in (13) and the corresponding CDW correlation function reads

$$\chi_0^{\text{cdw}} = -i \langle \mathcal{T} \hat{n}_{\mathbf{Q}} \hat{n}_{\mathbf{Q}} \rangle$$

which can be evaluated as

$$\chi_0^{\text{cdw}}(\omega) = \frac{4}{N} \sum_{\mathbf{k} \in \mathcal{B}_{0,\sigma}} \frac{\varepsilon_{\mathbf{k}}^2}{E_{\mathbf{k}}} \frac{f(E_{\mathbf{k}}^-) - f(E_{\mathbf{k}}^+)}{\omega^2 - 4E_{\mathbf{k}}^2}.$$

The interaction between the CDW fluctuations is given by  $V_{\mathbf{Q}} = 1/2(-\frac{|U|}{2})\delta\Delta_{\mathbf{Q}}\delta\Delta_{-\mathbf{Q}}$  so that the RPA result for the correlation function is obtained as

$$\chi^{\text{cdw}}(\omega) = \frac{\chi_0^{\text{cdw}}(\omega)}{1 - V_{\mathbf{Q}}\chi_0^{\text{cdw}}(\omega)}. \quad (\text{B9})$$

In particular, for  $\omega = 2\eta$ , i.e., at the energy of the CDW gap the denominator of Eq. (B9)

$$1 - V_{\mathbf{Q}}\chi_0^{\text{cdw}}(\omega) = 1 - \frac{|U|}{2N} \sum_{\mathbf{k} \in \mathcal{B}_{0,\sigma}} \frac{f(E_{\mathbf{k}}^-) - f(E_{\mathbf{k}}^+)}{E_{\mathbf{k}}} \quad (\text{B10})$$

vanishes when the external staggered field  $\alpha_{\mathbf{Q}} = 0$ . In fact, in this case Eq. (B10) is identical to the self-consistency equation for the CDW order parameter  $\eta_{CO}$ , so that for  $\alpha_{\mathbf{Q}} = 0$  the CDW amplitude excitations occur exactly at  $\omega = 2\eta_{CO}$  and therefore are damped due to their admixture with the quasiparticle excitations. With finite (positive)  $\alpha_{\mathbf{Q}}$  the amplitude excitation is further pushed into the continuum, however, since the real part of  $1 - V_{\mathbf{Q}}\chi_0^{\text{cdw}}(\omega)$  still acquires a minimum at  $\omega = 2\eta_{CO}$  the linear-response spectra in Fig. 10 are peaked at the energy of the CDW gap.

### Appendix C: Anharmonic oscillator: a classical example for out-of-equilibrium response functions

As a simple illustrative example we show results for a one-dimensional classical (anharmonic) oscillator. It is described by the differential equation

$$\ddot{x} = -x + \alpha x^3 + \Omega \sin(\omega t) \quad (\text{C1})$$

with ( $\Omega \neq 0$ ) or without ( $\Omega = 0$ ) an external frequency-dependent perturbation. We solve (C1) numerically in a time interval  $0 \leq t \leq \Delta t$  with the initial condition  $x(0) = x_0$  and  $\dot{x}(0) = 0$ . The solution with and without external perturbation are denoted as  $x_{\omega}(t)$  and  $x_0(t)$ , respectively. Like in the main part of this work, we define the time-dependent deviation

$$\delta x(t) = x_{\omega}(t) - x_0(t) \quad (\text{C2})$$

and its expectation value

$$\langle \delta x \rangle = \frac{1}{\Delta t} \int_0^{\Delta t} dt |x_{\omega}(t) - x_0(t)|, \quad (\text{C3})$$

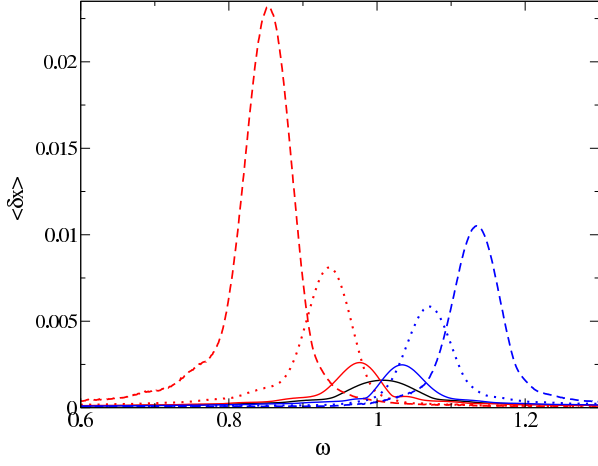


FIG. 16: Response function  $\langle \delta x \rangle$  of the anharmonic classical oscillator as a function of frequency  $\omega$  for  $\Omega = 10^{-4}$ ,  $\Delta t = 100$ ,  $\alpha = 1$  (red curves),  $\alpha = -1$  (blue) and initial amplitudes  $x_0 = 0.2$  (solid),  $x_0 = 0.4$  (dotted),  $x_0 = 0.6$  (dashed). For  $x_0 = 0$  the results for  $\alpha = 1$  and  $\alpha = -1$  are the same (black curve).

which is a function of the external frequency  $\omega$ . The expectation value (C3) serves as a measure of the system's response to the external perturbation.

In Fig. 16 we display  $\langle \delta x \rangle$  as a function of frequency around equilibrium ( $x_0 = 0$ ) and for several out-of-equilibrium amplitudes ( $x_0 \neq 0$ ). As expected, the peak position is shifted towards higher (lower) frequencies when  $\alpha = -1$  ( $\alpha = 1$ ). Out of equilibrium, the weight of the resonance grows substantially when the initial amplitude  $x_0$  is increased. This is in agreement with our corresponding observations for the negative  $U$  Hubbard model in the time-dependent Hartree Fock approximation. Note that in the linear limit ( $\alpha = 0$ ) the response function  $\langle \delta x \rangle$  is independent of the amplitude  $x_0$ , i.e., it is the same at and away from equilibrium. The frequency shifts and weight increases in Fig. 16 are therefore genuine effects of the non-linear terms in the differential equation (C1).

#### Appendix D: Two-site Hubbard model: exact solution versus Hartree-Fock approximation

The Hilbert space of a half filled two-site Hubbard model is four-dimensional when we assume that the total spin  $S_z$  in quantization direction is zero. A basis for this space may be chosen as

$$|d, 0\rangle = \hat{c}_{1,\uparrow}^\dagger \hat{c}_{1,\downarrow}^\dagger |\text{vac}\rangle, \quad (\text{D1})$$

$$|0, d\rangle = \hat{c}_{2,\uparrow}^\dagger \hat{c}_{2,\downarrow}^\dagger |\text{vac}\rangle. \quad (\text{D2})$$

$$|\uparrow, \downarrow\rangle = \hat{c}_{1,\uparrow}^\dagger \hat{c}_{2,\downarrow}^\dagger |\text{vac}\rangle, \quad (\text{D3})$$

$$|\downarrow, \uparrow\rangle = \hat{c}_{2,\uparrow}^\dagger \hat{c}_{1,\downarrow}^\dagger |\text{vac}\rangle. \quad (\text{D4})$$

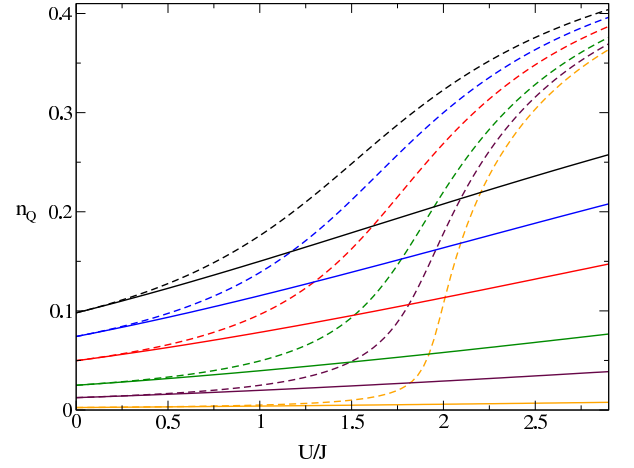


FIG. 17: Exact (solid lines) and Hartree-Fock (dashed lines) values for the charge density order  $n_Q$  in the ground state of the two site (negative  $U$ ) Hubbard model as a function of  $U/J$  and for  $\alpha_Q/J = 0.4$  (black), 0.3 (blue), 0.2 (red), 0.1 (green), 0.05 (maroon), 0.01 (orange).

When we want to study a pairing probe pulse we further need to include the states  $|0, 0\rangle = |\text{vac}\rangle$  and

$$|d, d\rangle = \hat{c}_{1,\uparrow}^\dagger \hat{c}_{1,\downarrow}^\dagger \hat{c}_{2,\uparrow}^\dagger \hat{c}_{2,\downarrow}^\dagger |\text{vac}\rangle \quad (\text{D5})$$

because the pairing operator  $\hat{\Delta}_0$  has the form

$$\hat{\Delta}_0 = \frac{-1}{2} \left[ |0, 0\rangle (\langle 0, d| + \langle d, 0|) + (|0, d\rangle + |d, 0\rangle) \langle d, d| \right]. \quad (\text{D6})$$

The charge density-operator  $n_Q$  in the two-site model is given as

$$\hat{n}_Q = \frac{1}{2} (|0, d\rangle \langle 0, d| - |d, 0\rangle \langle d, 0|). \quad (\text{D7})$$

At half filling, the chemical potential is  $\mu = -U/2$  and the operator  $\hat{K}$  hence becomes

$$\begin{aligned} \hat{K} = & J(\langle d, 0| + \langle 0, d|)(|\uparrow, \downarrow\rangle + |\downarrow, \uparrow\rangle) + \text{h.c.} \\ & + U(|\uparrow, \downarrow\rangle \langle \uparrow, \downarrow| + |\downarrow, \uparrow\rangle \langle \downarrow, \uparrow|) - \alpha_Q \hat{n}_Q. \end{aligned} \quad (\text{D8})$$

A Hartree-Fock approximation is particularly weak for low-dimensional systems. Hence, one cannot expect it to describe the physics of two-site Hubbard model satisfactorily. The difficulties are already visible in the ground state properties. In Fig. 17 we show the exact and Hartree-Fock values for the charge density order  $n_Q$  as a function of  $U/J$  and for several values of  $\alpha_Q$ . For  $\alpha_Q = 0$  the exact ground state shows no charge order whereas such an ordered state becomes stable in the Hartree Fock approximation for  $U/J > 2$ . This is due to the fact that a ‘doublet singlet state’ of the form  $|d, 0\rangle + |0, d\rangle$  becomes the ground state for  $U \gg J$  and cannot be described within the Hartree Fock approximation. For  $\alpha_Q \neq 0$  the exact and Hartree Fock results in

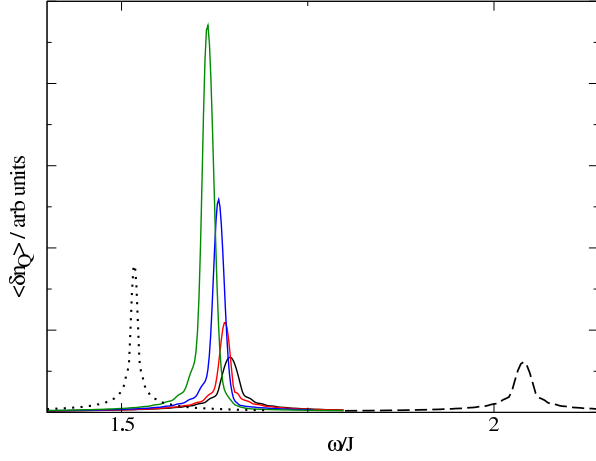


FIG. 18: Charge-order response  $\langle \delta n_{\mathbf{Q}} \rangle$  as a function of frequency for  $U/J = 1.5$  (dotted for exact and solid for TDHF results) and  $U/J = 0.0$  (dashed) with scaling factors  $\gamma = 1.0$  (black),  $\gamma = 0.8$  (red),  $\gamma = 0.6$  (blue), and  $\gamma = 0.4$  (blue).

Fig. 17 differ only quantitatively, however, these differences are quite substantial in large parts of the parameter space.

In the following we present pump-and-probe results for  $\alpha_{\mathbf{Q}} = 0.4$  where exact and Hartree Fock ground states show a finite charge order. We first consider the charge response function as it has been defined in the main text, see Eq. (48). The exact and TDHF results for  $\langle \delta n_{\mathbf{Q}} \rangle$  are displayed for  $U/J = 1.5$  and  $U/J = 0.0$  in Fig. 18 as a function of the probe frequency  $\omega$  and for several scaling factors  $\gamma$  (for the TDHF results). We show only one exact curve for each  $U$  because it appears to be largely

independent of the initial state at time  $t = 0$ . This is different from the Hartree-Fock curves which show a

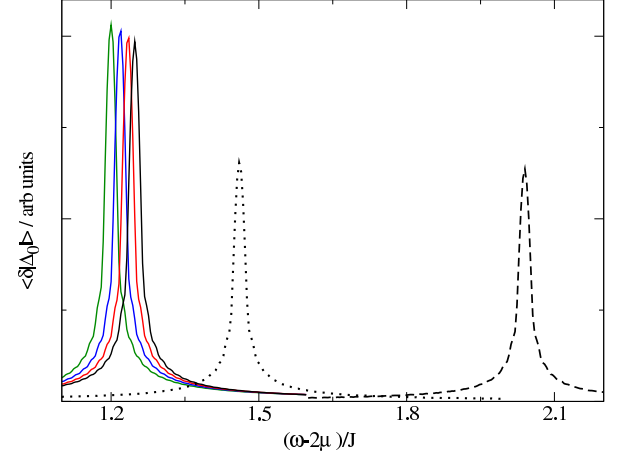


FIG. 19: Pairing response  $\langle \delta |\Delta_0| \rangle$  as a function of frequency for  $U/J = 1.5$  (dotted for exact and solid for TDHF results) and  $U/J = 0.0$  (dashed) with scaling factors  $\gamma = 1.0$  (black),  $\gamma = 0.6$  (red),  $\gamma = 0.4$  (blue), and  $\gamma = 0.2$  (blue).

shift towards smaller frequencies and a significant gain in spectral weight. The TDHF behavior of the two-site model therefore resembles that of the macroscopic systems which we investigate in the main text.

In Fig. 19 we show the corresponding results for the superconducting response function. Again, the exact curves are independent of the initial state. In this case, the TDHF shows a rather similar behavior. This, however, does not come as a surprise because it resembles our observations of the macroscopic systems in the main text.

<sup>1</sup> R. Kubo, J. Phys. Soc. Japan **12**, 550 (1957).

<sup>2</sup> R. Kubo, *Lectures in Theoretical Physics* (Wiley-Interscience, New York, 1959).

<sup>3</sup> G. D. Mahan, *Many Particle Physics* (Springer, Berlin, 2005).

<sup>4</sup> S. Dal Conte, C. Giannetti, G. Coslovich, F. Cilento, D. Bossini, T. Abebaw, F. Banfi, G. Ferrini, H. Eisaki, M. Greven, A. Damascelli, D. van der Marel, and F. Parmigiani, *Science* **335**, 1600 (2012).

<sup>5</sup> A. Pashkin, M. Porer, M. Beyer, K. W. Kim, A. Dubroka, C. Bernhard, X. Yao, Y. Dagan, R. Hackl, A. Erb, J. Demsar, R. Huber, and A. Leitenstorfer, *Phys. Rev. Lett.* **105**, 067001 (2010).

<sup>6</sup> Claudio Giannetti, Federico Cilento, Stefano Dal Conte, Giacomo Coslovich, Gabriele Ferrini, Hajo Molegraaf, Markus Raichle, Ruixing Liang, Hiroshi Eisaki, Martin Greven, Andrea Damascelli, Dirk van der Marel, and Fulvio Parmigiani, *Nature Commun.* **2**, 353 (2011).

<sup>7</sup> P. Kusar, V. V. Kabanov, J. Demsar, T. Mertelj, S. Sugai, and D. Mihailovic, *Phys. Rev. Lett.* **101**, 227001 (2008).

<sup>8</sup> Claudio Giannetti, Giacomo Coslovich, Federico Cilento, Gabriele Ferrini, Hiroshi Eisaki, Nobuhisa Kaneko, Martin

Greven, and Fulvio Parmigiani, *Phys. Rev. B* **79**, 224502 (2009).

<sup>9</sup> L. Perfetti, P. A. Loukakos, M. Lisowski, U. Bovensiepen, H. Eisaki, and M. Wolf, *Phys. Rev. Lett.* **99**, 197001 (2007).

<sup>10</sup> Nuh Gedik, Ding-Shyue Yang, Gennady Logvenov, Ivan Bozovic, and Ahmed H. Zewail, *Science* **316**, 425 (2007).

<sup>11</sup> Fabrizio Carbone, Ding-Shyue Yang, Enrico Giannini, and Ahmed H. Zewail, *Proc. Natl. Acad. Sci. U.S.A.* **105**, 20161 (2008).

<sup>12</sup> Barbara Mansart, Jos Lorenzana, Andreas Mann, Ahmad Odeh, Mariateresa Scarongella, Majed Chergui, and Fabrizio Carbone, *Proceedings of the National Academy of Sciences* **110**, 4539 (2013).

<sup>13</sup> J. Lorenzana, B. Mansart, A. Mann, A. Odeh, M. Chergui, and F. Carbone, *The European Physical Journal Special Topics* **222**, 1223 (2013).

<sup>14</sup> Y. D. Chuang, W. S. Lee, Y. F. Kung, A. P. Sorini, B. Moritz, R. G. Moore, L. Patthey, M. Trigo, D. H. Lu, P. S. Kirchmann, M. Yi, O. Krupin, M. Langner, Y. Zhu, S. Y. Zhou, D. A. Reis, N. Huse, J. S. Robinson, R. A. Kaindl, R. W. Schoenlein, S. L. Johnson, M. Först, D. Doering,

- P. Denes, W. F. Schlotter, J. J. Turner, T. Sasagawa, Z. Hussain, Z. X. Shen, and T. P. Devereaux, Phys. Rev. Lett. **110**, 127404 (2013).
- <sup>15</sup> W. S. Lee, Y. F. Kung, B. Moritz, G. Coslovich, R. A. Kaindl, Y. D. Chuang, R. G. Moore, D. H. Lu, P. S. Kirchmann, J. S. Robinson, M. P. Minitti, G. Dakovski, W. F. Schlotter, J. J. Turner, S. Gerber, T. Sasagawa, Z. Hussain, Z. X. Shen, and T. P. Devereaux, Phys. Rev. B **95**, 121105 (2017).
- <sup>16</sup> M. Först, R. I. Tobey, H. Bromberger, S. B. Wilkins, V. Khanna, A. D. Caviglia, Y.-D. Chuang, W. S. Lee, W. F. Schlotter, J. J. Turner, M. P. Minitti, O. Krupin, Z. J. Xu, J. S. Wen, G. D. Gu, S. S. Dhesi, A. Cavalleri, and J. P. Hill, Phys. Rev. Lett. **112**, 157002 (2014).
- <sup>17</sup> M. Först, A. Frano, S. Kaiser, R. Mankowsky, C. R. Hunt, J. J. Turner, G. L. Dakovski, M. P. Minitti, J. Robinson, T. Loew, M. Le Tacon, B. Keimer, J. P. Hill, A. Cavalleri, and S. S. Dhesi, Phys. Rev. B **90**, 184514 (2014).
- <sup>18</sup> Claudio Giannetti, Massimo Capone, Daniele Fausti, Michele Fabrizio, Fulvio Parmigiani, and Dragan Mihailovic, Advances in Physics **65**, 58 (2016).
- <sup>19</sup> R. Mankowsky, M. Först, and A. Cavalleri, Rep. Prog. Phys. **79**, 064503 (2016).
- <sup>20</sup> G. De Filippis, V. Cataudella, E. A. Nowadnick, T. P. Devereaux, A. S. Mishchenko, and N. Nagaosa, Phys. Rev. Lett. **109**, 176402 (2012).
- <sup>21</sup> Davide Rossini, Rosario Fazio, Vittorio Giovannetti, and Alessandro Silva, EPL (Europhysics Letters) **107**, 30002 (2014).
- <sup>22</sup> Zala Lenarčič, Denis Golež, Janez Bonča, and Peter Prelovšek, Phys. Rev. B **89**, 125123 (2014).
- <sup>23</sup> Can Shao, Takami Tohyama, Hong-Gang Luo, and Hantao Lu, Phys. Rev. B **93**, 195144 (2016).
- <sup>24</sup> L. P. Kadanoff and G. Baym, *Quantum statistical mechanics* (W. A. Benjamin, New York, 1962).
- <sup>25</sup> L. V. Keldysh, Zh. Eksp. Teor. Fiz. **47**, 1515 (1964).
- <sup>26</sup> Hideo Aoki, Naoto Tsuji, Martin Eckstein, Marcus Kollar, Takashi Oka, and Philipp Werner, Rev. Mod. Phys. **86**, 779 (2014).
- <sup>27</sup> M. Schiro and M. Fabrizio, Phys. Rev. Lett. **105**, 076401 (2010).
- <sup>28</sup> M. Schiro and M. Fabrizio, Phys. Rev. B **83**, 165105 (2011).
- <sup>29</sup> J. Büneemann, M. Capone, J. Lorenzana, and G. Seibold, New J. Phys. **10**, 053050 (2013).
- <sup>30</sup> Y. F. Kung, W.-S. Lee, C.-C. Chen, A. F. Kemper, A. P. Sorini, B. Moritz, and T. P. Devereaux, Phys. Rev. B **88**, 125114 (2013).
- <sup>31</sup> P. Ring and P. Schuck, *The Nuclear Many-Body Problem* (Springer-Verlag, New York, 1980).
- <sup>32</sup> J.-P. Blaizot and G. Ripka, *Quantum Theory of Finite Systems* (MIT Press, Cambridge, MA, 1986).
- <sup>33</sup> R. Micnas, J. Ranninger, and S. Robaszkiewicz, Rev. Mod. Phys. **62**, 113 (1990).
- <sup>34</sup> R. A. Barankov, L. S. Levitov, and B. Z. Spivak, Phys. Rev. Lett. **93**, 160401 (2004).
- <sup>35</sup> T. Papenkort, V. M. Axt, and T. Kuhn, Phys. Rev. B **76**, 224522 (2007).
- <sup>36</sup> T. Papenkort, T. Kuhn, and V. M. Axt, Phys. Rev. B **78**, 132505 (2008).
- <sup>37</sup> H. Krull, D. Manske, G. S. Uhrig, and A. P. Schnyder, Phys. Rev. B **90**, 014515 (2014).
- <sup>38</sup> Alireza Akbari, Andreas P. Schnyder, Dirk Manske, and Ilya Eremin, EPL (Europhysics Letters) **101**, 17002 (2013).
- <sup>39</sup> A. F. Volkov and Kogan Sh. M., Zh. Eksp. Teor. Fiz. **65**, 2038 (1973).
- <sup>40</sup> Emil A. Yuzbashyan, Oleksandr Tsypliyatyev, and Boris L. Altshuler, Phys. Rev. Lett. **96**, 097005 (2006).
- <sup>41</sup> T. Cea and L. Benfatto, Phys. Rev. B **90**, 224515 (2014).
- <sup>42</sup> F. Bashforth and J. C. Adams, *An attempt to test the theories of capillary action by comparing the theoretical and measured forms of drops of fluid : with an explanation of integration employed in construction of integrating the tables which give the theoretical forms of such drops* (Cambridge University Press, Cambridge, 1883).
- <sup>43</sup> S. R. Manmana, S. Wessel, R. M. Noack, and A. Muramatsu, Phys. Rev. Lett. **98**, 210405 (2007).
- <sup>44</sup> Martin Eckstein, Marcus Kollar, and Philipp Werner, Phys. Rev. B **81**, 115131 (2010).
- <sup>45</sup> Simone A. Hamerla and Götz S. Uhrig, Phys. Rev. B **87**, 064304 (2013).
- <sup>46</sup> Simone A. Hamerla and Götz S. Uhrig, Phys. Rev. B **89**, 104301 (2014).
- <sup>47</sup> Johannes Bauer, Mehrtash Babadi, and Eugene Demler, Phys. Rev. B **92**, 024305 (2015).
- <sup>48</sup> Naoto Tsuji, Martin Eckstein, and Philipp Werner, Phys. Rev. Lett. **110**, 136404 (2013).
- <sup>49</sup> H. Krull, B. Bittner, G.S. Uhrig, D. Manske, and A.P. Schnyder, Nature Communications **7**, 11921 (2016).
- <sup>50</sup> T. Cea, C. Castellani, G. Seibold, and L. Benfatto, Phys. Rev. Lett. **115**, 157002 (2015).
- <sup>51</sup> P. W. Anderson, Phys. Rev. **130**, 439 (1963).
- <sup>52</sup> N. Bergeal, J. Leseueur, M. Aprili, G. Faini, J. P. Contour, and B. Leridon, Nature Physics **4**, 608 (2008).
- <sup>53</sup> P. André, M. Schiró, and M. Fabrizio, Phys. Rev. B **85**, 205118 (2012).
- <sup>54</sup> M. Fabrizio, in *New Materials for Thermoelectric Applications: Theory and Experiment*, edited by V. Zlatić and A. Hewson A. (Springer, Dordrecht, 2013).
- <sup>55</sup> M. Sandri and M. Fabrizio, Phys. Rev. B **88**, 165113 (2013).
- <sup>56</sup> G. Seibold, J. Büneemann, and J. Lorenzana, J. Supercond. Nov. Magn. **27**, 929 (2014).
- <sup>57</sup> J. Büneemann, S. Wasner, E.v. Oelsen, and G. Seibold, Philosophical Magazine **95**, 550 (2015).